Quaternary Science Reviews 253 (2021) 106770

Contents lists available at ScienceDirect

Quaternary Science Reviews

journal homepage: www.elsevier.com/locate/quascirev

Quaternary record of terrestrial environmental change in response to climatic forcing and anthropogenic perturbations, in Puerto Rico

Emma J. Harrison [a, b, *], Jane K. Willenbring [a, b], Gilles Y. Brocard [c]

[a] Scripps Institution of Oceanography, UC San Diego, La Jolla, CA, USA
[b] Now at Department of Geological Sciences, Stanford University, Stanford, CA, USA
[c] Archéorient, UMR 5133, Maison de l'Orient et de la Méditerranée, University of Lyon 2, France

ARTICLE INFO

Article history:
Received 21 February 2020
Received in revised form
8 December 2020
Accepted 14 December 2020
Available online xxx

Keywords:
Quaternary
Environmental change
Vegetation dynamics
Paleoerosion
Caribbean
Cosmogenic isotopes
Carbon isotopes

ABSTRACT

We present cospatial, contemporary archival records of biotic and abiotic terrestrial processes operating over the past ~25 ky within the Rio Fajardo watershed, in northeastern Puerto Rico. The proxy records were derived from a 5-m-thick stratigraphic section exposed by cut bank incision. We interpreted ecosystem dynamics from changes in the stable carbon isotopic ratio of sedimentary organic material compared to δ^{13}C ratios of contemporary carbon sources. Sedimentary organic material had δ^{13}C values ranging from −29.715 to −15.291. We derived a record of paleo-erosion rates in the catchment from the concentration of meteoric ^{10}Be in layers of the floodplain sediments. Paleo-erosion rates ranged from 13 to 356 mm ky^{-1}. The chronology of the sediments was constrained with the radiocarbon ages of organic deposits, the oldest age was calibrated to ~22.4 ky BP (thousand years before present) and retrieved at 440 cm depth. We collected grain size data, clay mineralogies, and analyzed geochemical indices including the chemical weathering index, salinization, and base cation loss down profile. This stratigraphic sequence captures major shifts in the Caribbean climate, the intensification of the El Nino-Southern Oscillation, and the arrival of humans on the island. During the last glacial and early Holocene epochs both biotic (δ^{13}C) and abiotic proxies (^{10}Be$_{met}$ and geochemical data) indicated dynamic equilibrium with climate. The past five thousand years (ky) of record are characterized instead by pulsed responses to disturbances in both systems. Colonial-era land use drove changes that significantly exceeded natural variability in any proxy over the period of record.

© 2020 Elsevier Ltd. All rights reserved.

1. Introduction

The future climate of the Caribbean is projected to have more extreme seasonality and increased frequency of tropical storm impacts (Karmalkar et al., 2013; Campbell et al., 2011; Angeles et al., 2007). How these changes will impact the terrestrial environment where we live, and the ecosystems on which we depend, are important questions. We present proxy records of terrestrial change from the Caribbean spanning ~25 ky of the late Quaternary — a time period during which global climate changed dramatically. From the late Pleistocene to the Holocene, there was a general trend in the Caribbean towards a warmer, wetter climate (Bradbury 1997; Fensterer et al., 2013; González and Gómez 2002) increasingly influenced by the El Niño-Southern Oscillation (ENSO) (Donnelly and Woodruff 2007; Woodruff et al., 2008) although temperature and precipitation proxies show significant spatial variation (Leyden et al., 1994; Metcalfe et al., 1997; Haug et al., 2011). In addition, human occupation of Puerto Rico began as early as 5.5 ky BP (Burney et al. 1994) and Spanish colonization 500 years BP brought widespread, intensive anthropogenic land clearing and monocrop agriculture (Thomlinson et al., 1996).

Biotic and abiotic surface processes are joint regulators of global-scale biogeochemical cycling. Carbon cycle models forecasting scenarios of anthropogenic climate change are driven by weathering/erosion and biotic uptake/release (Sarmiento and Gruber 2002). Rates of change and the response sensitivity of these systems are areas of active debate (Herman and Champagnac 2015; Norton and Schlunegger, 2017; Willenbring and Jerolmack 2015). These systemic drivers respond to external forcing by the climate, but they also change in reaction to each other. Vegetation is hypothesized to regulate rates of geomorphic processes (e.g. Collins

* Corresponding author.
E-mail addresses: ejharris@ucsd.edu (E.J. Harrison), willenbring@stanford.edu (J.K. Willenbring), gilles.brocard@mom.fr (G.Y. Brocard).

https://doi.org/10.1016/j.quascirev.2020.106770
0277-3791/© 2020 Elsevier Ltd. All rights reserved.

et al., 2004; Lyell and Deshayes, 1830) and landscape evolution can change ecosystem composition and structure (e.g. Wolf et al., 2016; Brocard, Willenbring and Scatena, 2019). Although sedimentary archives are valued tools for predictive modeling (Franklin et al., 2016) there are few instances where archives of terrestrial landscapes and ecosystems have been studied together (Marshall et al., 2015). When the external forcing changes significantly, do ecosystems and surface processes respond in sync, out of sync, or are they unresponsive? By tracing contemporaneous changes in the landscape and ecology of a single watershed we can investigate when proxies are correlated and differences in the style or timescale of response to external perturbations.

We present two proxy records from the floodplain stratigraphy of the Rio Fajardo (Fig. 1) in northeastern Puerto Rico. Floodplain sediments accumulated from ~25 ky BP to the present and contain temporally and spatially coincident proxies of geomorphic activity and ecosystem composition. Basin-wide erosion rates were calculated from measurements of meteoric ^{10}Be concentrations in detrital sediment from radiocarbon-dated stratigraphic layers. Ecological change was inferred from stable carbon isotope ratios in sedimentary organic carbon. Both proxy records contained periods of quiescence, of gradual change, and of dramatic changes attributable to external forcing. We found that the abiotic and biotic systems in this watershed were dynamic and responsive to the regional climate and the human history of the island.

1.1. Sedimentary archives of ecogeomorphology

Sediments accumulate on floodplains when rivers overtop their banks, and, unconfined by the channel walls, the flow spreads out and slows. Suspended sediment settles out of the low-velocity flow and deposits on the floodplain. Over time, this process leads to accumulated layers of sediment with the composition of the suspended load. The thickness and frequency of deposits laid down in floodplain stratigraphy is modulated by climate (Aalto et al., 2003), changes in the sediment supply in the upstream watershed (Swanson et al., 2008), and by sea-level trends (Aslan and Autin 1999). Deposited sediments are likely to be retained because floodplains occupy low gradient spaces with low surface erosion rates. However, all sedimentary records are incomplete, and their completeness decreases with depth of time due to the stochastic nature of depositional processes. Sediment is transported in pulses through fluvial channels (Ashmore 1991; Singh et al., 2009) and the cumulation of hiatuses in the sediment flux increases with the age of the depositional record (Schumer and Jerolmack 2009; Jerolmack and Sadler 2007). Nevertheless, sedimentary archives provide unparalleled access into Earth's environmental, climatic and biological evolution (Berger et al. 1981).

River suspended loads include particulate organic carbon from plant litter and soil. Organic carbon contains distinct isotopic signatures that are characteristic of different types of organic matter (O'Leary 1988). Stable carbon isotopic ratios (δ^{13}C) of organic

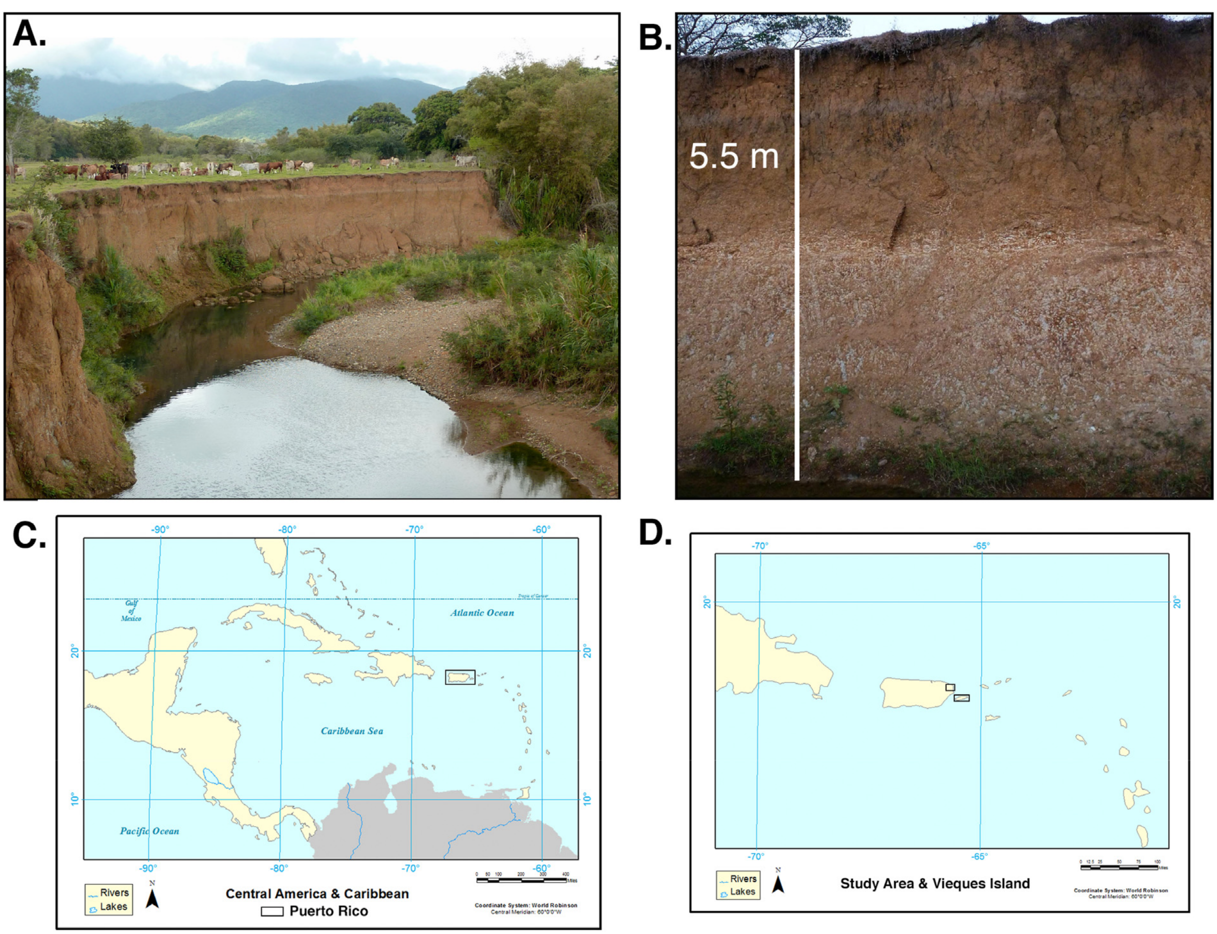

Fig. 1. AImage of the Rio Fajardo floodplain exposed by river incision with cows for scale. Several meters of river incision over recent decades (Clark and Wilcock 2000) have exposed the floodplain stratigraphic section sampled for this study. **B.** A close-up photograph of the profile that was sampled for analysis. **C.** Map of the Caribbean with Puerto Rico and Vieques Island identified by a bold box, adapted from (Wood et al., 2019).

material distinguish plant groups by their photosynthetic mechanism (Smith and Epstein 1971). C_3 type plants (trees and shrubs) $\delta^{13}C$ ratios typical range is from $-26.5\ ^0/_{00}$ to $-28.0\ ^0/_{00}$ (O'Leary 1988; Tieszen 1991). C_4 type plants (including some tropical grasses) incorporate more ^{13}C, the "heavier" carbon isotope, and have $\delta^{13}C$ values falling between $-12.5\ ^0/_{00}$ and $-14.0\ ^0/_{00}$ (O'Leary 1988; Tieszen 1991). Agricultural crops common to the Caribbean, such as sugarcane, use the C_4 pathway (Tieszen 1991). Terrestrial pools of organic matter (e.g. soil OM) have $\delta^{13}C$ values that integrate the isotope ratios of carbon inputs. The organic carbon transported by rivers has a $\delta^{13}C$ ratio that represents a mixture of the biomass in the watershed (Thurman 2012; Hedges et al., 2000; Hedges et al. 1984). As plant communities within the watershed shift, the changing ecosystem is reflected in the $\delta^{13}C$ ratios of organic material actively transported in the river. $\delta^{13}C$ has been used to assess the relative contribution of C_3 and C_4 plants to riverine organic matter in many global rivers (Cai et al. 1988; Bird et al., 1992; Onstad et al., 2000; Louchouarn et al. 1999; Louchouarn et al., 1997). Sedimentation of particulate organic material in floodplains preserves the history of ecological change within a watershed (Planavsky et al. 2016; Kohn 2010).

Cosmogenic $^{10}Be_{met}$ ($t_{1/2}$ = 1.39 My) is produced in the atmosphere and delivered to Earth's surface with precipitation (Lal and Peters 1967). The nuclide binds tightly to soil particles in the near surface (>1 m), creating a reservoir that accumulates in proportion to the stability of the soil (Willenbring and von Blanckenburg 2010a,2010b). The erosion rate of a surface is calculated as the inverse of the $^{10}Be_{met}$ concentration (von Blanckenburg, Bouchez, and Wittmann 2012; Willenbring and von Blanckenburg 2010a,2010b; Jungers et al., 2009) if the meteoric deposition rate of $^{10}Be_{met}$ is known, and the site variables that may disassociate the nuclide from mineral surfaces can be assessed. $^{10}Be_{met}$ has been widely applied as an erosion tracer in soils (Graly et al., 2010) on hillslopes (Jungers et al., 2009), the active load in river sediments (Reusser and Bierman 2010), and marine sediments (Willenbring and von Blanckenburg, 2010b). However, this tracer has rarely been applied in terrestrial sedimentary contexts, where the $^{10}Be_{met}$ concentration in the each depositional layer contains an archived paleoerosion record (Jagercikova et al., 2015; Marshall et al., 2015).

2. Field setting

Rio Fajardo forms in the Luquillo Mountains in northeastern Puerto Rico, then flows east to the Vieques Sound, an inlet body of the Atlantic Ocean. The bedrock lithologies are primarily interbedded volcanoclastic rocks and Quaternary alluvium filling the coastal plain (Fig. 2C) (Bawiec, 1999). The total catchment area is

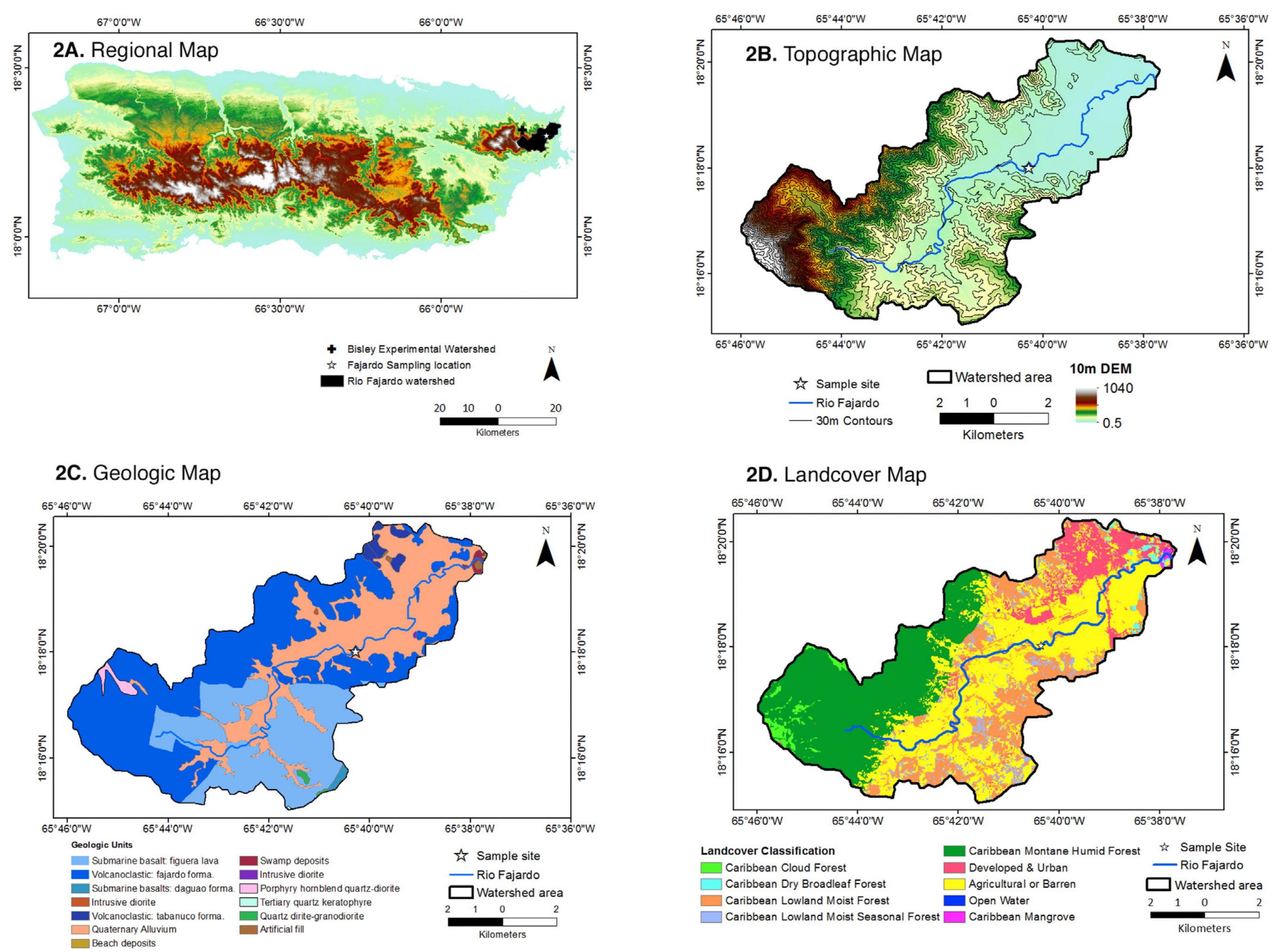

Fig. 2. Four maps of the Fajardo watershed area. **A**. A regional relief map of Puerto Rico with the area of the Fajardo watershed identified. **B**. A topographic map of the Fajardo watershed with 30-m contour lines and the location of the sampling site identified. **C**. Geologic map of the Rio Fajardo watershed adapted from (Walter J. Bawiec 1999). **D**. Landcover units for the Rio Fajardo watershed adapted from (Homer et al., 2004).

~70 km^2. Rainfall in the headwaters is as high as 4500 mm/year and decreases to around 1500 mm/year along the coast (Murphy et al., 2017). Vegetation is zoned by elevation (Fig. 2D). The headwaters and mountain reaches are primary forest Tabanuco, Palo Colorado and Sierra Palm forest (Lugo and Helmer, 2004). Along the coastal plain, the ecosystem today is largely abandoned pasture that has been reforested, with a portion remaining active cropland and pasture (Lugo and Helmer 2004). The watershed delta is a developed urban area (USGS, 2001). Roughly 60% of the land area is dominated by C_3 type plants with $\delta^{13}C$ ratios between −26 and −30 $^o/_{oo}$ (von Fischer and Tieszen 1995). Nearly a third is actively cleared lands with mixed C_3 and C_4 species (Lugo and Helmer 2004). These areas host an abundance of C_4 type plants whose $\delta^{13}C$ ratios range from −11 to −15 $^o/_{oo}$ (Salomé et al., 2010; Medina et al. 1991; Medina et al., 1999).

3. Methods

3.1. Sampling strategy and site characterization

Our sampling location (65.670997°N, 18.300754°W) was within a broad floodplain of the Fajardo river, 25 m above sea level. The site today is primarily pasture. We sampled a cut bank exposure of ~5.5 m of sediment above a layer of rounded to sub-angular, poorly sorted basalt cobbles. The profile was initially sampled for radiocarbon ages, geochemical indices, grain size, and $\delta^{13}C_{org}$ in 1997, and re-sampled in 2015 for $^{10}Be_{met}$. Radiocarbon sampling was done at 40 cm intervals between the surface and 200 cm depth, with one basal age collected at 440 cm depth. Grain size, clay mineralogies, and elemental composition were measured for samples collected at either 10 or 20 cm intervals from the surface to 520 cm depth. Stable carbon isotopes were measured in samples collected at 10 cm intervals between 20 cm and 140 cm depth, then at a spacing of 20 cm between 140 cm and 520 cm depth. $^{10}Be_{met}$ was sampled at approximately 20 cm intervals between the surface and 520 cm depth.

3.2. Radiocarbon dating

The chronology of the floodplain stratigraphy was established using radiocarbon measurements of bulk organic material collected from the exposure. Samples were measured for ^{14}C at the University of Arizona Accelerator Mass Spectrometer (AMS) laboratory (Table 1) and previously reported in Mellon (2000). The samples were graphitized and their $^{14}C/^{12}C$ ratios were measured via AMS. We used the Bayesian calibration and age-modeling program *Bchron* (Haslett and Parnell 2008; Parnell et al., 2008) to generate an age depth model (Fig. 3) and probability distributions for each radiocarbon age (Fig. 4) using the calibration curve IntCal20 (Reimer et al., 2020).

3.3. Stable carbon isotopes

Stable carbon isotopes of organic material in the floodplain were finely ground and sent for processing and analysis at the Mountain Mass Spectrometry laboratory in Evergreen, Colorado (n = 22, 500 mg each). Replicates were sent for eight of the measurements to the University of Arizona for comparative analysis. Samples were measured for $\delta^{13}C_{org}$ using a Dumas combustion technique, in which combustion products are passed through a series of chemical and cryogenic traps to isolate the CO_2 gas. A helium carrier was used to transport the gas to the mass spectrometer ion source for analysis. Five replications had a precision of 0.2 per mil. Results are reported in δ PDB notation (Table 3):

Table 1
Calibrated radiocarbon ages and interpolated age of the floodplain.

Lab ID	Depth	^{14}C years	+/−	Calibrated Age[a]
	M	years BP	years BP	years BP
AA24059	0.2	450	40	448 ± 4 (89.2%) 344 ± 11 (3.6%)
AA24060	0.6	1325	55	1245 ± 70 (70.8%) 1330 ± 10 (17.4%) 1143 ± 20 (4.8%) 1086 ± 6 (1%)
AA24061	0.8	1910	60	1827 ± 121 (80%) 1974 ± 14 (14.5%)
AA24062	1.2	3920	160	4397 ± 427 (94.1%) 3936 ± 6 (0.6%)
AA24063	1.6	5340	65	6136 ± 144 (92.5%) 5954 ± 7 (2%)
AA24064	1.9	8975	65	10072 ± 169 (94.4%)
AA24067	4.4	18380	210	22378 ± 506 (94.7%)

[a] Calibrated ages summing to 95% of the highest density regions determined from a Bayesian age-depth model (Fig. 4) with the software Bchron (Parnell et al., 2008).

$$\delta^{13}C_{org} = \left[\left(R_{sample} - R_{std}\right) \Big/ R_{std}\right] \times 100 \tag{1}$$

3.4. Meteoric ^{10}Be concentrations

Chemical extraction of ^{10}Be was performed in the University of Pennsylvania Cosmogenic Isotope Laboratory following procedures described in Valletta et al. (2015). A ^9Be carrier (Supplier Purdue Rare Isotope Measurement Laboratory) with a $^{10}Be/^9Be$ ratio of $0.5 \pm 0.1 \times 10^{-15}$ was added to each sample. The $^{10}Be/^9Be$ ratio of the samples was measured by accelerator mass spectrometry at PRIME Laboratory, Purdue University. Results were normalized to the 07KNSTD standard (Nishiizumi et al., 2007) with an assumed $^{10}Be/^9Be$ ratio of 2.79×10^{-11} (Balco et al., 2009).

Erosion rates were calculated following (Willenbring and von Blanckenburg, 2010a):

$$E = \frac{Q}{\rho N_{surf}} \tag{2}$$

where E is an erosion rate (cm y^{-1}) that averages erosion rates from the contributing areas of the watershed at the time the given sedimentary sequence was being deposited in the floodplain; we use a value of 8.70 E+05 (atoms cm^{-2} yr^{-1}) for Q, the flux of $^{10}Be_{met}$, which we assume to be constant on the timescale of soil ages in the catchment (Willenbring and von Blanckenburg, 2010a); ρ is a density term for which we use an average value of 1.59 g cm^{-3} and N_{surf} is the measured concentration of $^{10}Be_{met}$ extracted from the sediment sample. We use the sampling latitude to derive the $^{10}Be_{met}$ flux predicted by General Circulation Models (Heikkilä et al., 2013; Heikkilä and von Blanckenburg 2015). Global datasets of $^{10}Be_{met}$ fluxes do not show unlimited supply in high precipitation environments (Willenbring and von Blanckenburg, 2010a) therefore, we do not use a precipitation-scaled flux rate (Graly et al. 2011). We account for the impact of $^{10}Be_{met}$ fallout on the surface of the floodplain using aggradation rates of 0.02 and 0.06 cm/year based on the modeled accumulation rates (Fig. 4B). Erosion rates accounting for this in situ flux differ by <0.01%.

3.5. Grain size and geochemistry

Samples were measured for their grain size distribution, clay mineralogies, and elemental composition. Macromorphological

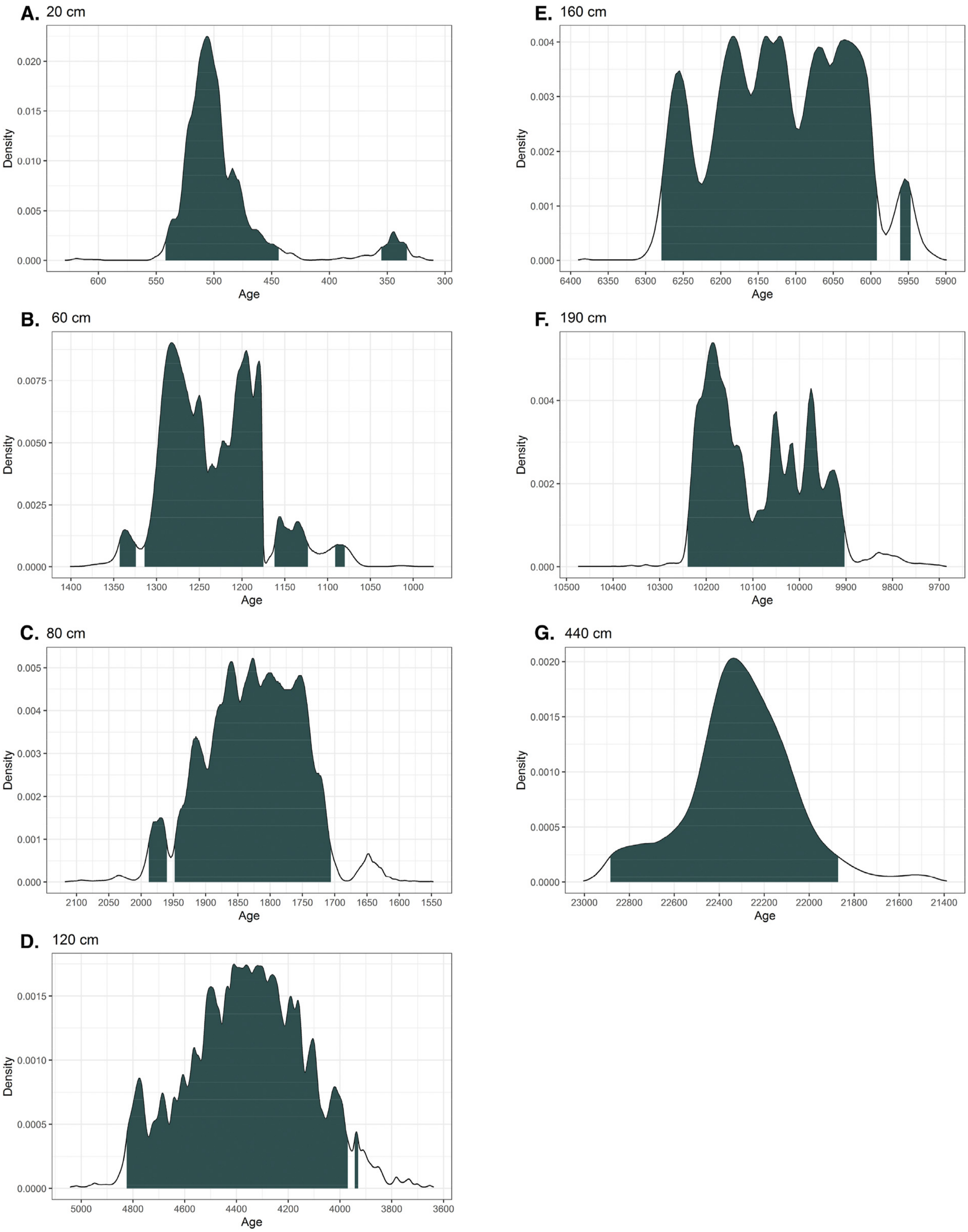

Fig. 3. Probability distributions for ages calibrated using a Bayesian age-depth modeling software *Bchron* and the ^{14}C calibration curve IntCal20. Shaded regions sum to 95% of all possible date calibrations. Shaded regions correspond to calibrated ages reported in Table 1. **A.** Sample collected 20 cm below the surface. **B.** Sample collected 60 cm below the surface. **C.** Sample collected 80 cm below the surface. **D.** Sample collected 120 cm below the surface. **E.** Sample collected 160 cm below the surface. **F.** Sample collected 190 cm below the surface. **G.** Sample collected 440 cm below the surface.

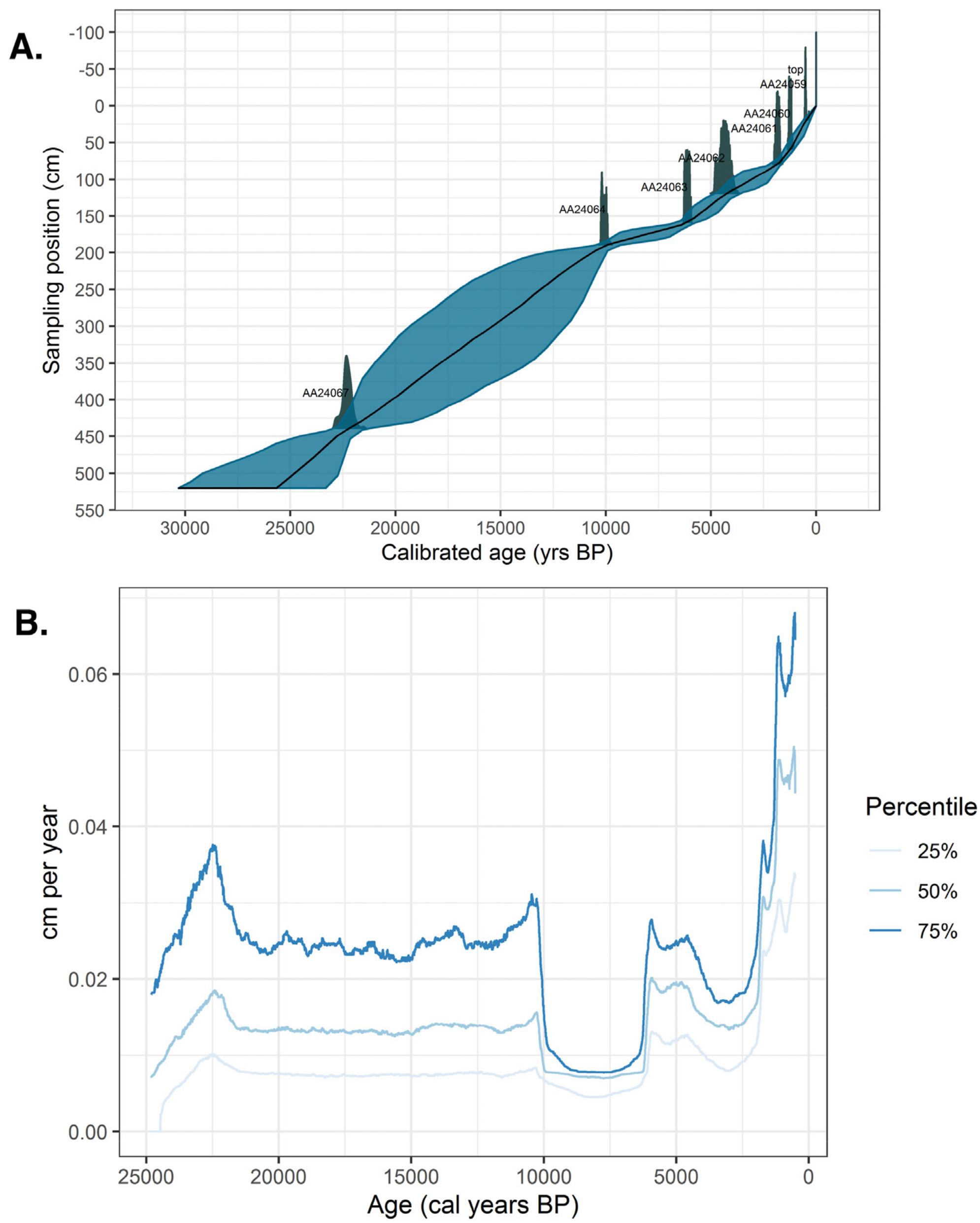

Fig. 4. Age-depth model and accumulation rates determined for the Fajardo floodplain cutbank exposure. **A.** Age depth model showing sampling depth (cm) on the y-axis and calibrated age in years BP on the x-axis. Blue shaded region represents the 95% highest posterior density regions showing the uncertainty of the ages assigned to samples between dated layers. Black line shows the median age. Probability distributions are shown for each sample (see Fig. 3) and are labeled with the AMS lab number. **B.** Accumulation rate (cm yr^{-1}) over time derived from the age-depth model. Quantiles are given. (For interpretation of the references to color in this figure legend, the reader is referred to the Web version of this article.)

observations of horizons include texture, structure, the presence of roots and voids, and grain coatings (Fig. 5). Elemental concentrations were measured in triplicate with a PerkinElmer Emission Spectrometer Plasma 400 ICP AES after total digestion with lithium metaborate and lithium tetraborate. Canadian Certified Reference Materials Soil-2, Soil-3, and Soil-4 were used as standards. Samples with high Fe and Si were diluted to 1:2 and 1:5 concentration respectively. Standards were within 5–10% of reported values. Results are presented as ratios calculated to show the relative degree of change throughout the profile (Fig. 5). Calculated weathering ratios are the base cation loss (Retallack 2008) the chemical index of weathering (Harnois 1988) and salinization.

$$\text{Base cation loss } = Al_2O_3/(CaO + MgO + Na_2O + K_2O) \tag{3}$$

$$\text{Chemical Weathering Index} = [Al_2O_3 \,/\, (Al_2O_3 + CaO + Na_2O)] \times 100 \tag{4}$$

$$\text{Salinization} = \mathrm{Na}_2O \,/\, K_2O \tag{5}$$

The percent weight of three grain size fractions (sand, silt, clay) were determined for each sampling interval using settling columns to separate fractions, where were subsequently dried and weighed following procedures described in Lewis and McConchie (1994).

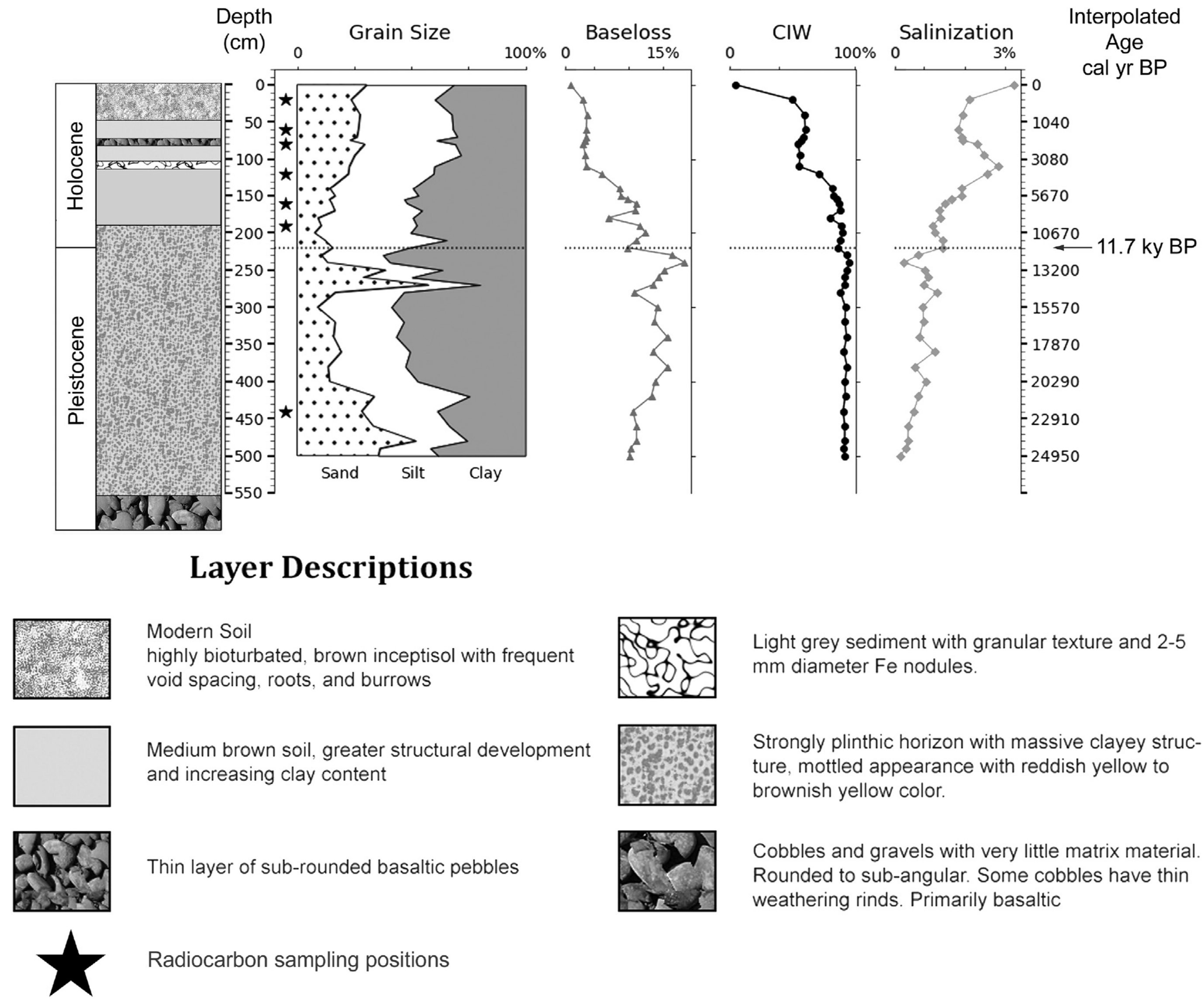

Fig. 5. Stratigraphy plotted along with the position of radiocarbon sampling and down-profile data on grain size distributions, base loss, chemical index of weathering, and salinization. Median calibrated age from the age-depth model is given for the depth positions between 0 and 550 cm at 50 cm intervals. A dotted line denotes the Pleistocene to Holocene transition 11.7 ky BP.

4. Results

4.1. Stratigraphy and chronology

The top 50 cm of the sediment column was bioturbated, medium-brown and fine grained with voids and roots present (Mellon, 2000). Below 50 cm—~200 cm depth, sediments were yellow-brown to yellow-orange with a moderately columnar to blocky structure and greater clay concentration. Two distinct but narrow bands in the deposit (see Figs. 1 and 5) existed within this 50 cm—200 cm section. A one-pebble thick layer of sub-rounded basalt pebbles (D_{50} = 4.5 cm) was 80 cm below the surface, continuing horizontally for the length of the exposure. The lithology of this pebble band was consistent with the rounded cobbles at the base of the cut bank exposure. At a depth of 100 cm was a 20 cm thick band of sediment with a light grey color exhibiting a small number of 2—5 mm diameter Fe-nodules. From 200 cm to the cobble deposit at 550 cm the exposed profile was strongly plinthic, highly weathered and Fe-rich, with a high clay content and massive structure (Mellon, 2000).

We interpreted the chronology of the floodplain deposits using the Bayesian age-depth modeling software *Bchron* and the ^{14}C calibration curve IntCal20. *Bchron* calculates probability distributions for radiocarbon ages (Fig. 3, Table 1) given a user-specified calibration curve, and then fits a compound Poisson-Gamma distribution to increments between dated positions (Haslett and Parnell 2008; Parnell et al., 2008). The largest uncertainty envelope exists between the base of the stratigraphic column (550 cm) and the radiocarbon sample at 190 cm depth (10,072 ± 169 cal yr BP) as there is only a single radiocarbon age (440 cm depth, 22378 ± 506 cal yr BP) constraining this segment of the stratigraphy. In general, the stratigraphy did not suggest any long hiatuses in deposition or significant erosion of the surface. There was no evidence of buried soil horizons, the color and geochemical indices of the sediment show little variation with depth (Fig. 5), and grain size distributions were similar for most of the profile (Fig. 5).

In *Bchron*, segments are modeled piecewise, which allows for abrupt changes in modeled accumulation rates (Fig. 4B). The age-depth model implied a steady accumulation rate from the basal age (22.4 ky BP, 440 cm depth) until approximately 10 ky BP (190 cm depth). This section of the stratigraphy corresponds to a very consistent plinthite layer (Fig. 5). Modeled accumulation rates dropped over the next segment, representing 30 cm of sediment and ~4 ky (next dated sample is collected at 160 cm depth with a calibrated age of ~6 ky BP). Modeled accumulation rates were variable from 6 ky BP to the present but increased overall. The modeled rate rose above the rates determined for the plinthite layer ~4 ky BP and continued to climb until the present.

4.2. Grain size and geochemistry

Two anomalies were present in the grain size distribution: a sandier unit at ~260 cm depth and a thin layer of pebbles deposited 80 cm below the modern surface (Fig. 5). Radiocarbon dating indicates that the sandy layer was deposited between ~13 and 14 ky BP. Deposition of the layer of sub-rounded basalt pebbles at ~80 cm depth is dated to 1.8 ky BP. In this section of the river, we observed some braiding and splitting of the river channel – and so consider it is possible that these stones were laid down by a smaller channel briefly flowing over the floodplain before being integrated into the main stem. An event like this could potentially affect the depositional record, however, the lithology of the pebbles is the same material actively transported in the modern channel and forming the cobble deposit at the base of the floodplain. Therefore, we are confident that the source material entering the deposit should be derived from the same region.

4.3. Erosion rates from $^{10}Be_{met}$

Erosion rates (Table 2, Fig. 8) calculated from $^{10}Be_{met}$ concentrations (Table 2, Fig. 5) during the Last Glacial Maximum (considered here as interpolated ages from 24.6 to 21.7 ky BP) have a minimum value of 69 ± 1.2 mm ky^{-1} and a maximum of 93 ± 1.3 mm ky^{-1}. Erosion rates decreased at 21.7 ky BP to 52.5 ± 1.0 mm ky^{-1} and reached a minimum of 13.4 ± 0.3 mm ky^{-1} at 12.4 ky BP just prior to the Holocene transition. Early Holocene erosion rates were modest, with a maximum of 79 ± 1.8 mm ky^{-1} at 11.3 ky BP and showed little variability until ~4.3 ky BP. At that time, erosion more than doubled to 135 ± 2.7 mm ky^{-1} and remained high into the present. In this later time period, erosion rates fluctuated between measured intervals, peaking at 356 ± 16 mm ky^{-1}, 470 years BP. The most recent erosion rate measured from the exposed surface was 111 ± 1.6 mm ky^{-1}.

Table 3
Stable carbon isotopes of sedimentary organic carbon.

Interpolated Age[a] cal yr BP	Depth m	$\delta^{13}C$ Mountain Mass Spectrometry	$\delta^{13}C$ University of Arizona
500	0.2	−17.275	−15.291
860	0.4	−21.39	
1240	0.6	−24.805	−21.332
1540	0.7	−24.97	
1850	0.8	−22.265	
2470	0.95	−21.66	
3690	1.1	−20.615	
4330	1.2	−19.465	−19.776
5220	1.4	−23.62	
6140	1.6	−24.265	−21.136
8750	1.8	−22.155	
10,060	1.9	−24.09	−24.372
11,650	2.2	−23.38	
12,690	2.4	−25.6	
13,630	2.6	−24.945	−29.715
15,440	3	−25.875	
17,370	3.4	−26.07	
19,2230	3.8	−26.28	
22,290	4.4	−25.59	−26.846
23,910	4.8	−24.753	
24,280	4.9	−25.82	
25,900	5.2	−26.135	−27.103

[a] Median of calibrated age probability distributions rounded to the nearest decade, shown as a black line in Fig. 4A.

Table 2
$^{10}Be_{met}$ in floodplain sediments and calculated erosion rates.

PRIME lab #	Sample depth m	Interpolated age[b] cal yr BP	^{10}Be concentration atoms g^{-1}	AMS uncertainty	Erosion rate[a] mm ky^{-1}
201202860	0	0	4.92 E+07	1.48%	111 ± 2
201202861	0.13	320	2.47 E+07	1.71%	222 ± 4
201202862	0.19	470	1.54 E+07	4.55%	356 ± 16
201202863	0.44	940	2.72 E+07	2.21%	201 ± 4
201202864	0.69	1510	3.63 E+07	2.08%	151 ± 3
201202865	0.95	2770	6.66 E+07	1.59%	82 ± 1
201202866	1.2	4330	4.05 E+07	2.00%	135 ± 3
201202867	1.38	5140	1.07 E+08	1.50%	51 ± 1
201202868	1.55	5870	1.18 E+08	1.32%	46 ± 1
201202869	1.73	7830	9.24 E+07	1.71%	59 ± 1
201202870	1.9	10,060	9.48 E+07	1.64%	58 ± 1
201202871	2.12	11,270	6.94 E+07	2.27%	79 ± 2
201202872	2.34	12,380	4.09 E+08	2.61%	13 ± 0
201202873	2.56	13,450	1.39 E+08	2.36%	39 ± 1
201202874	2.78	14,460	1.51 E+08	1.24%	36 ± 0
201202875	3.0	15,440	2.54 E+08	1.28%	22 ± 0
201202876	3.22	16,470	1.22 E+08	1.07%	45 ± 0
201202877	3.44	17,570	1.26 E+08	3.64%	43 ± 2
201202878	3.66	18,490	1.41 E+08	0.98%	39 ± 0
201202879	3.88	19,610	1.41 E+08	0.97%	39 ± 0
201202880	4.1	20,220	1.51 E+08	1.22%	36 ± 0
201202881	4.32	21,730	1.04 E+08	1.82%	53 ± 1
201202882	4.54	22,980	7.32 E+07	1.12%	75 ± 1
201202883	4.76	23,770	5.86 E+07	1.35%	93 ± 1
201202884	4.98	24,600	7.89 E+07	1.68%	69 ± 1
201202885	5.2	24,640	6.42 E+07	1.67%	85 ± 1

[a] Calculated with equation (2), rounded to whole numbers.
[b] Median of calibrated age probability distributions rounded to the nearest decade, shown as a black line in Fig. 4A.

4.4. Stable carbon isotope ratios

For the Pleistocene-age samples (considered here as interpolated ages from 23.9 ky to 12.7 ky BP) the average $\delta^{13}C$ value was −26.28 $^{o}/_{oo}$ with a standard deviation of 1.36, reflecting a relatively stable biomass structure. There was much greater variability during the Holocene, $\delta^{13}C$ values range from −23.38 $^{o}/_{oo}$ in the first Holocene sample (11.7 ky BP, 2.2 m depth) to −15.291 $^{o}/_{oo}$ (500 yr BP, 20 cm depth). $\delta^{13}C$ values closer to 1 reflect greater incorporation of the carbon isotope ^{13}C. There were several time periods in this record exhibiting distinct trends, listed in Table 6 in the discussion. The replicate measurements at the University of Arizona were generally in good agreement with the measurements made at the Mountain Mass Spectrometry Lab, but in one case (260 cm depth, 13.63 ky BP) deviated by a significant value (4.77 $^{o}/_{oo}$). This variability may represent either differences in the lab processing or variability between separates from the same depositional layer of the floodplain.

5. Discussion

5.1. $^{10}Be_{met}$ as a paleo-erosion proxy

Interpreting paleo-erosion rates from floodplain sediments assumes that the $^{10}Be_{met}$ concentration of suspended sediment is a valid representation of the average erosion in the river catchment today. To interrogate this, we used the nearby Bisley watershed as an analogue because it is underlain by the same volcanoclastic bedrock formation and has been studied for decades as part of the Luquillo Experimental Forest (Scatena, 1989). To accurately calculate soil residence time, $^{10}Be_{met}$ must be retained in the near surface. Whether it exists as a hydroxide compound or as an organic complex, Be binds tightly to sediment where the environmental pH is greater than four (Willenbring and von Blanckenburg, 2010a; You et al., 1989). Spatially extensive measurements of soil pH in the Bisley watershed ranged from 4.7 to 5.3 (Silver et al., 1994) which suggests Be retention. We measured $^{10}Be_{met}$ in a surface soil (0−10 cm) and in a sample exposed by a landslide scar (160−170 cm) to look for evidence of leaching or translocation. The surface soil $^{10}Be_{met}$ concentration was an order of magnitude higher than the landslide exposure (Table 4).

The Bisley surface soil yielded an erosion rate approximately double that of the measurement from the top ten cm of the Fajardo floodplain. This is reasonable, because the Bisley soil represents a point measurement from the steep mountain peaks, whereas Rio Fajardo at the floodplain integrates a significant area of lowlands. High rates of chemical erosion in a Bisley weathering profile likewise reflect the difference in mass loss on the peaks compared to lower in the watershed (Dosseto et al. 2012). In June of 2011 we collected water from Rio Bisley during the early stages of a flood event. We separated suspended sediment using a 0.7 μm filter and measured the concentration of $^{10}Be_{met}$ for the suspended load. The yield was similar to the modern floodplain deposit, suggesting that $^{10}Be_{met}$ concentrations are a valid approximation for catchment-averaged erosion in the watershed today.

Floodplain accumulation is an inherently selective process that preferentially retains small particles. We explored the bias introduced by sorting during entrainment to determine whether floodplain settings can be meaningful paleo-erosion proxies. The first question is whether the sub-sample of sediment retained in the floodplain carries a $^{10}Be_{met}$ concentration that is representative of the suspended sediment population as a whole. Willenbring and von Blanckenburg (2010a) measured $^{10}Be_{met}$ variability within size fraction populations, finding a tight distribution of $^{10}Be_{met}$ concentrations in small size fractions. Furthermore, Boschi and Willenbring (2021)measured the strength of Be sorption under a range of conditions, and found that grain size was among the least important variables in sorption capacity. Clay mineral abundances and total % clay in our samples did not co-occur with high concentrations of $^{10}Be_{met}$ (Fig. 6) suggesting minimal $^{10}Be_{met}$ redistribution (Boschi and Willenbring 2021) following deposition in the floodplain. The two peaks in $^{10}Be_{met}$ concentration occurred at approximately 10 and 13.4 ky BP (depth intervals of 190 cm and 256 cm respectively). These concentrations do not correspond to anomalously low erosion rates. The erosion rate data contained one high outlier, sampled at 19 cm depth, above a layer of grey-colored sediment. Erosion rates increased towards the top of the profile within the modern soil layer, however, based on the consistency of the clay composition and our assessment of $^{10}Be_{met}$ mobility under the specific field conditions, we do not interpret this increase as being controlled by the sediment composition.

Table 4
$^{10}Be_{met}$ concentrations in Bisley watershed soils and active channel.

Site description	Sampling strategy	$^{10}Be_{met}$ atoms g^{-1}	AMS Uncertainty
Fajardo floodplain sediment	0−10 cm	4.92 E+07	1.48%
Surface soil in Bisley	0−10 cm	2.46 E+07	3%
Landslide scar in Bisley	160−170 cm	5.52 E+06	28%
Bisley suspended sediments	1.7 ft flood stage	2.65 E+08	2%

5.2. Carbon sources and ecological succession

Pools of organic matter, such as are stored in soils or sediments, have $\delta^{13}C$ ratios that integrate the $\delta^{13}C$ values of source material. Decomposition further fractionates these isotopic ratios, such that the $\delta^{13}C$ value of the bulk material becomes more like the $\delta^{13}C$ of the recalcitrant fraction. Marin-Spiotta et al. (2009) reported measurements of Puerto Rican soil organic matter in primary and successional stand forests and agricultural fields to quantify the outcome of microbial decomposition and humification on bulk $\delta^{13}C$ ratios. Litter in primary forests contained high-density, decomposition-resistant fractions that were depleted in ^{13}C relative to low-density, quickly-recycling organic matter. With time, aging bulk SOM $\delta^{13}C$ progressed towards the ^{13}C depleted, heavy-fraction component. $\delta^{13}C$ ratios of Tabanuco forest living biomass and litter from von Fischer and Tieszen (1995) show the same trend of old litter being ^{13}C depleted relative to wood and roots. Marin-Spiotta et al. (2009) found the opposite pattern in pastures, reflecting different inputs of organic carbon.

Decomposition rate and the residence times of organic soils on hillslopes can vary greatly within a given watershed, and often correlates with the local erosion rate. A study of riverine organic carbon in active transport along the Rio Fajardo channel found that the $\delta^{13}C$ of particulate carbon changed downstream (Moyer et al. 2013). Carbon in the river headwaters was dominated by forest litter and soil organic matter. Downstream, where the watershed area contains more agriculture and grassland, the river integrated a larger percentage of ^{13}C-enriched sources. Their study found that organic carbon in the headwaters had modern radiocarbon ages due to short soil residence times and fast erosion on steep mountain slopes. At the downstream sampling location a few tens of meters away from our floodplain site, particulate organic carbon was mostly modern with a maximum age of ~200 years. Young particulate organic carbon in the active channel reduces several uncertainties associated with carbon archived in the floodplain. It suggests minimal alteration of $\delta^{13}C$ ratios by decomposition prior to

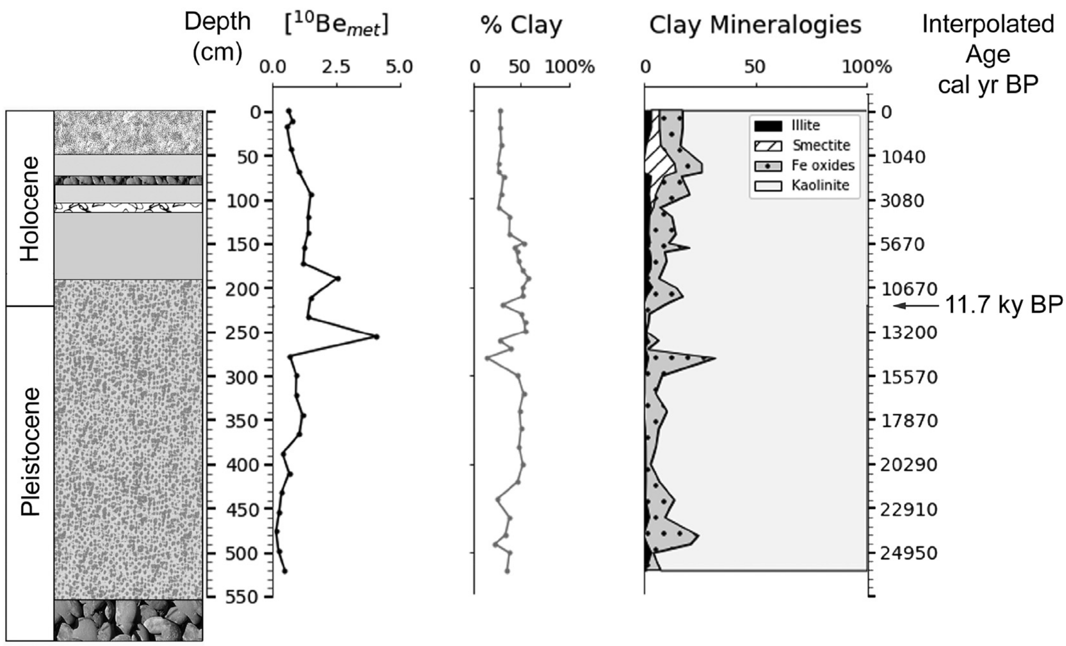

Fig. 6. Distribution of $^{10}Be_{met}$ concentration, percent clay, and clay mineral abundances. $^{10}Be_{met}$ concentrations are in 10^8 atoms gram^{-1}. Total clay and the abundance of clay minerals are plotted as a percentage of the total mass. The peak in ^{10}Be is at 256 cm depth and the minimum percent clay and maximum percent Fe-oxides is at 280 cm depth.

fluvial transport. Also, that radiocarbon ages were probably modern, or close to it, when the carbon was entrained in the floodplain. Decomposition is slow within floodplain sediments due to anoxia, which promotes preservation of organic carbon (Boye et al., 2017). Oxidation of organic material during fluvial transport and transient storage is documented for large watersheds (Galy et al. 2008; Bouchez et al., 2010) but Rio Fajardo is a small, steep catchment where carbon is unlikely to degrade during transport in the channel (Scheingross et al., 2019).

We compared the $\delta^{13}C$ values of sedimentary organic matter in the Fajardo floodplain to carbon sources in the Fajardo watershed (Fig. 7). Pleistocene-age organic carbon (calibrated ages between 25.9 and 12.7 ky BP) overlapped tightly with the $\delta^{13}C$ of forest biomass, litter, and soil organic matter. There was only a narrow

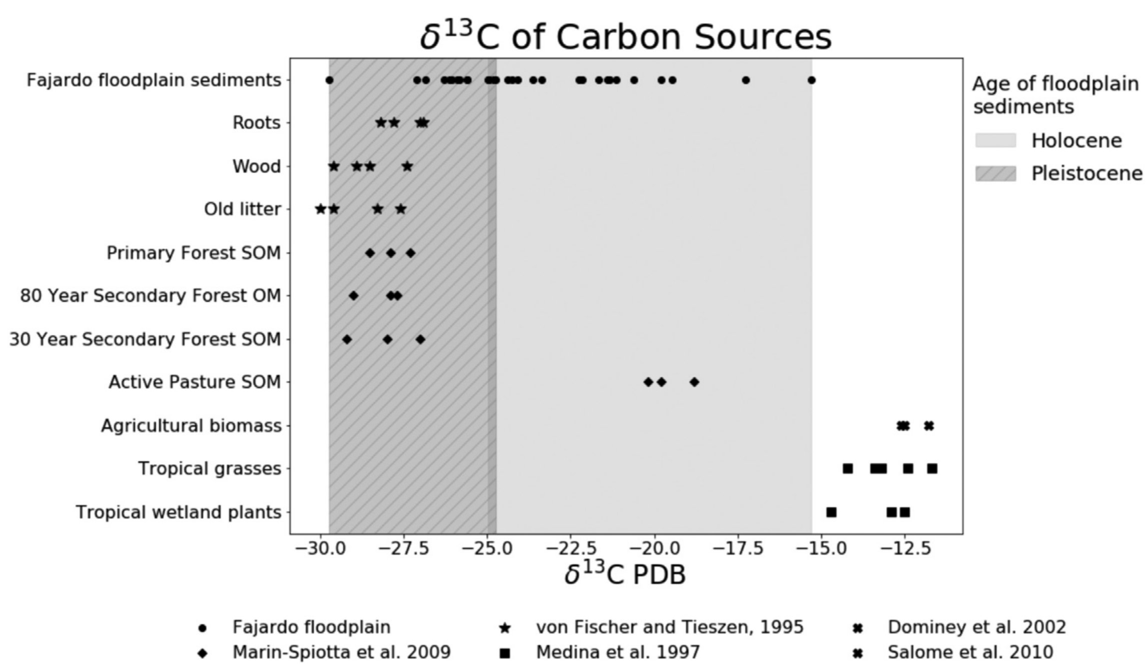

Fig. 7. $\delta^{13}C$ ratios of organic carbon that potentially source the material transported by Rio Fajardo. The $\delta^{13}C$ distribution of the samples collected from the Fajardo floodplain are plotted, and the radiocarbon calibrated ages of the carbon are indicated by the shaded regions. Light grey shading represents the extent of $\delta^{13}C$ values for organic material of Holocene age. Grey shading with hatch marks indicates the range of $\delta^{13}C$ values for organic carbon of Pleistocene age. Plotted $\delta^{13}C$ values represent forest biomass (von Fischer and Tieszen 1995), aged soil organic matter (Marin-Spiotta et al., 2009), agricultural soils (Salomé et al., 2010; Dominy et al. 2002), tropical grasses and sedges (Medina et al., 1999), and floodplain sediments (this study).

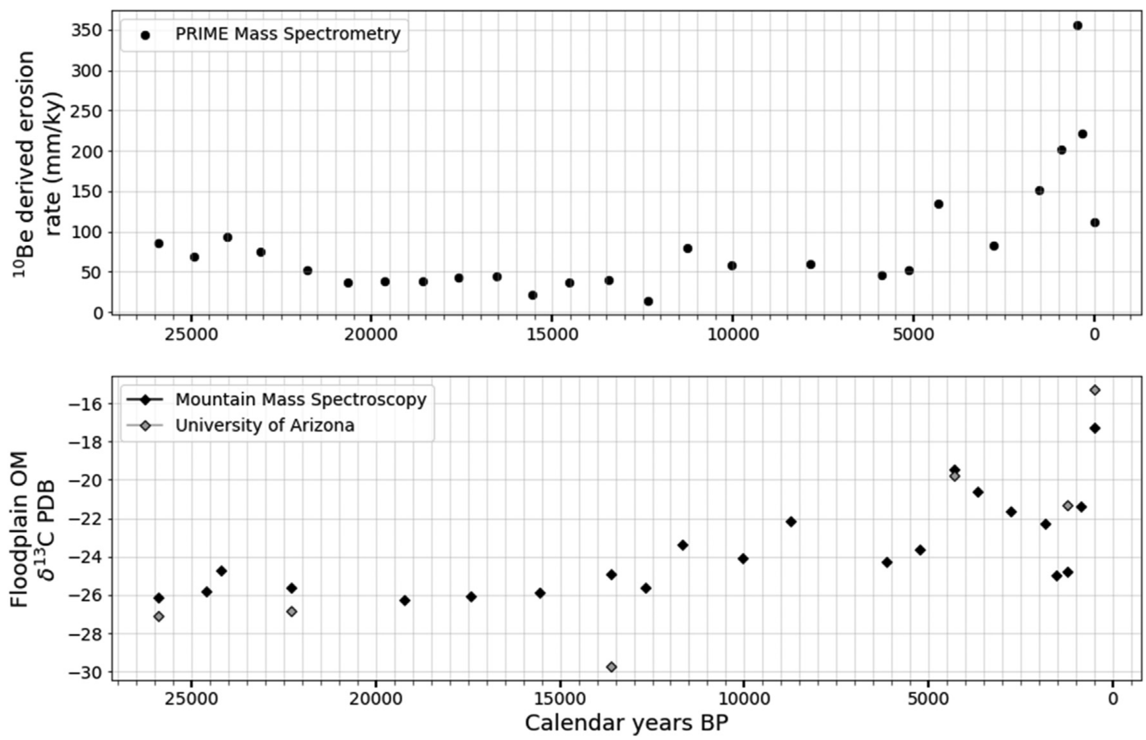

Fig. 8. Age calibrated measurements of paleoerosion rates (top) derived from $^{10}Be_{met}$ concentrations and $\delta^{13}C$ ratios of organic material (bottom) retrieved from the sedimentary record of the Rio Fajardo floodplain.

band of overlapping $\delta^{13}C$ values between Pleistocene and Holocene-age sedimentary carbon. All Holocene-age samples had significantly higher $\delta^{13}C$ ratios than samples from the Pleistocene. Climate change can affect the $\delta^{13}C$ of plants because they respond to changing water availability and temperature with behaviors that affect their carbon uptake during photosynthesis (Farquhar et al. 1989; O'Leary 1988). The $\delta^{13}C$ of most C_3 plants increases slightly as the plant responds to increased temperature and aridity. The effect of glacial/interglacial climates is capable of producing intra-species variations of ~2 $^{o}/_{oo}$ (Heaton 1999). The differences between Pleistocene and Holocene age carbon in the Fajardo floodplain is greater than this value, indicating new biomass derived from C_4 plants. The magnitude of change is evidence that the pattern shown in Fig. 8 is ecological succession occurring in the Fajardo watershed over time.

5.3. Chronology of terrestrial change

The ~25 ky Fajardo floodplain record demonstrates that terrestrial systems responded in concert with external perturbations (Fig. 8). In the earliest part of the record, between 25–22 ky ago, abiotic and biotic environmental proxies showed low magnitude variability that could reflect climatic excursions or be caused by stochasticity in the collection, transport, and retention of eroded material in fluvial and floodplain systems. Over the remainder of the last glacial period (22–12.6 ky BP) both records had extremely low variability. Erosion rates were well below the modern rates, averaging 50 mm ky^{-1}. The $\delta^{13}C$ of organic material was within the range of the modern forest biomass for the same period. At the end of the Pleistocene (11.7 ky BP), trends in the two records began to diverge. The $\delta^{13}C$ record started shifting gradually higher with a greater rate of change. The simultaneous record of erosion increased modestly but remained stable. Quiescence and gradual change were replaced in both records by dynamic fluctuations ~4.3 ky ago. Erosion rates more than doubled, peaking ~470 years ago, and remaining high into the present. The $\delta^{13}C$ record began to change sharply between sampling horizons, becoming lower (more like the Tabanuco forest) then dramatically higher (dominated by tropical grasses and wetlands). The highest values in the record were deposited approximately 500 years BP, coincident with the peak in erosion. Both proxies diverged increasingly from their previous norms from 4.3 ky BP to the present, suggesting that external perturbations became more powerful in the late Holocene.

5.4. Caribbean paleoclimate and environmental change

Paleoclimate proxy records spanning the Quaternary indicate that the Caribbean region was sensitive to climate perturbations in North America and the northern Atlantic (Peterson and Haug 2006; Haug et al., 2011). Generally, the transition from the Pleistocene to the Holocene (~11.7 ky BP) marks increasing temperatures and humidity across the Caribbean (Bradbury 1997; González and Gómez 2002; Fensterer et al., 2013; Hodell et al., 1991; Haug et al., 2011) although the Caribbean is characterized by a complex mosaic of microclimates (Bradbury 1997; Leyden et al., 1994). At the annual scale, climate variability is driven by the ENSO cycle (Giannini et al. 2001). During El Niño years, the trade winds are stronger, sea surface temperatures cooler, and seasonality is more extreme in the Caribbean and tropical Atlantic Ocean (Giannini et al. 2001). A dramatic uptick in ENSO activity at ~5 ky BP is indicated by modeling studies (Clement et al. 2000), geo-archaeological evidence (Sandweiss et al., 1996), and paleoclimate reconstructions from proxy data (Rodbell et al., 1999). Proxy records spanning the last several hundred years are dominated by anthropogenic impacts (Peten et al., 1998; Islebe et al., 1996; Huang et al., 2001; Bradbury 1997).

Extreme weather from tropical storm systems and hurricanes are central components of the modern Caribbean climate and have massive impacts on ecosystems and on geomorphic processes. ENSO cycles drive the frequency and intensity of hurricanes (Tartaglione, Smith, and O'Brien 2003) and there is strong evidence that hurricane landfalls in eastern Puerto Rico increased beginning 5 ky BP (Donnelly and Woodruff 2007; Woodruff et al., 2008). Numerical models of atmospheric circulation during the Last Glacial Maximum have found that if hurricanes did form in the tropical Atlantic at that time, they would have been substantially less powerful than contemporary storms (Hobgood and Cerveny 1988). Growth structures of Pleistocene age coral reefs in the Caribbean indicate minimal impacts by major storms as compared to younger reefs (Meyer et al., 2003; Giry et al., 2012). Individual hurricane landfalls in lagoon deposits on Vieques Island, ~30 km southeast of the Fajardo delta, show the same temporal pattern (Woodruff et al., 2008).

Anthropogenic land-use also restructures ecosystems and alters geomorphic processes. There are many examples of impactful land cover change by pre-colonial peoples in the Caribbean region (Peten et al., 1998; Burney et al. 1994; Koch et al., 2019). However, there are no known archaeological excavations within the floodplain area, and the Luquillo Mountains were regarded as sacred by the Taino people (Scatena, 1989) who inhabited Puerto Rico at the time of European colonization. Historic land use, however, has completely restructured the terrestrial landscape of the Rio Fajardo watershed. Sugar cane cultivation began in 1498, and an aerial photographic survey shows that the region was intensely developed as agricultural fields or pastures in 1936 (Thomlinson et al., 1996). In the 1950's agricultural land use declined, and by 1988 a repeat aerial survey found the majority of the landscape had been reforested (Thomlinson et al., 1996). Mining in the Luquillo Mountains occurred between the 14th and 19th centuries and kilns for industrial and personal charcoal production were constructed (Scatena, 1989). Changing land use and coarsening sediment supply is believed to have enhanced river incision over the last decade (Clark and Wilcock 2000) which likely exposed the floodplain stratigraphic section sampled in this study.

5.5. Patterns in erosion

We considered the Fajardo floodplain archive in four timeframes: glacial, late-glacial, early Holocene, and mid-Holocene to the present day (Table 5). We drew a distinction between the glacial and late glacial periods of the Pleistocene due to a large decrease in the averages of erosion rates from 75 ± 1 mm ky^{-1} (glacial) to 35 ± 1 mm ky^{-1} (late glacial). This may be a representation of precipitation trends driven by global climate cycles. Over the Quaternary, cyclic glacial stadials and interstadials have been identified from the changing $\delta^{18}O$ of foraminifera. The transition from an interstadial phase (warmer climate) to a stadial phase (cooler climate) (Lisiecki and Raymo 2005) occurred just prior to decreasing erosion rates in the Fajardo watershed (20.2 ky BP). Low erosion rates persisted until the calibrated age position of 4.3 ky BP, thereafter becoming distinctly greater in both magnitude and variability, which we posit is evidence of changing external perturbations (Scatena et al., 2012).

Until the mid-Holocene, erosion rates changed modestly in a manner that tracked the general trend of regional climatic conditions. This trend could be explained mechanistically by the link between river discharge and sediment transport capacity (e.g. DiBiase and Whipple, 2011). Positive correlations between precipitation and long-term erosion rates have been documented in landscapes that are in dynamic equilibrium with respect to rock uplift (Ferrier et al., 2013; Reiners et al., 2003). Bedrock weathering and the production of mobile regolith also depends on rates of mean annual precipitation (Owen et al., 2011; Dixon et al., 2009). However, research compiling multiple study areas finds no dependence of denudation on mean annual temperatures or precipitation (Riebe et al. 2004; von Blanckenburg 2005). In the context of this single watershed, bedrock composition and fracture density are constants, and a stable base level position is indicated by the watershed geomorphology (Pike et al. 2010) and geochemical tracers of surface lowering (Dosseto et al. 2012). Therefore, climate is the most likely driver of changes in the paleoerosion archive. While erosion in the Rio Fajardo was apparently responsive to climate change, it acted as a low-pass filter of climate oscillations, responding to fluctuations at timescales larger than 1–3 ky.

In the most recent 4.3 ky of record, the average erosion rate was more than double any time over the preceding 20 ky. Temporally, this behavior aligns with the onset of ENSO-driven hurricanes as a disturbance regime in eastern Puerto Rico (Donnelly and Woodruff 2007; Woodruff et al., 2008). High precipitation during extreme weather increases slopewash and surface erosion (Larsen et al., 1999) and is key to triggering landslides. Mass wasting events occur when thresholds in soil pore-pressure are exceeded, which is directly linked to the intensity and duration of rainfall (Larsen and Simon, 1993). The impacts of modern hurricanes provide insight into the dependence of long-term erosion rates on hurricane landfalls. Larsen and Sanchez (1992) documented more than 400 landslides triggered in the Luquillo Mountains by Hurricane Hugo in 1989. In the Rio Fajardo watershed, the landside density was 10 per km^2 after the same hurricane. The authors determined a recurrence interval for long-duration/high-intensity storms using historic precipitation data and calculated a storm-triggered average erosion rate of 164 mm ky^{-1} for the Luquillo Mountains (Larsen and Torres Sanchez, 1992; Larsen and Torres-Sanchez, 1998). This value is extremely close to the 180 mm ky^{-1} average since the mid-Holocene indicated by the $^{10}Be_{met}$ proxy record. Erosion rates dependent on landslide frequency and a hurricane-driven disturbance regime agrees with the results of geomorphic studies in the Luquillo Mountains that use other methodologies (Brown et al., 1995; Larsen et al., 1999; Stallard, 2012). Soil salinization is a major impact of hurricane landfalls, and has been documented in the Luquillo Mountains and adjacent coastal plain areas following hurricanes (Lodge and McDowell 1991; Gardner et al., 1992). Our measurements of soil geochemistry show a major spike in salinization during the past 5 ky (Fig. 5), providing corroborative evidence for increased frequency of storm surges and saltwater delivered in tropical storms. Geochemical weathering proxies also

Table 5
Erosion rate changes over the Fajardo floodplain stratigraphic record.

Time frame	Date range[a] ky BP	Average ε mm ky^{-1}	Coefficient of variance	Maximum change[b] mm ky^{-1}
Mid-Holocene to present	0–4.3	180 ± 5	47%	155
Early-Holocene	5.1–11.3	59 ± 1	19%	−65
Late Glacial	12.4–20.2	35 ± 1	28%	23
Glacial	21.7–24.6	75 ± 1	19%	−24

[a] Date ranges are delineated by interpolated radiocarbon ages of sampled horizons (see Table 2).
[b] Greatest difference in calculated erosion rate between sampling horizons.

showed a change after 5 ky BP. Materials deposited after this time were less weathered, which could reflect a greater prevalence of landslides eroding deeper and chemically fresher portions of the weathering profile.

The extremely high erosion rate of 356 ± 16 mm ky^{-1} calibrated to approximately 470 years BP was most likely driven by land use change within the watershed. Erosion rates from agricultural fields globally are 1–2 orders of magnitude higher than erosion under native vegetation and measured by long-term proxies (Montgomery 2007). Intensive agricultural and pastoral land use likely drove watershed erosion rates well above the pre-colonial level (Scatena, 1989). Recent reforestation in the watershed, likewise, may have contributed to the subsequent lowering of erosion rates (Aide et al. 1995, 1996, 2000).

5.6. Patterns in the ecosystem

The $\delta^{13}C$ of sedimentary organic matter had an overall tendency towards higher values and specific trends within time frames (Table 6). We did not distinguish between late glacial ages for these samples, because the mean and standard deviation of the sample populations did not change between those intervals. Pleistocene-age $\delta^{13}C$ values were constant, recording no inferred shift in the ratio between C_3 and C_4 plants over this interval. The average $\delta^{13}C$ during the last glacial maximum (-26.23 ‰) suggested little biomass derived from C_4 plants. The $\delta^{13}C$ distribution was extremely tight if we remove one outlier (-29.72 ‰) giving an average $\delta^{13}C$ of -25.91 ‰, a standard deviation of 0.7 ‰, and a 3% coefficient of variance. Differences between sample intervals in the Pleistocene (excepting the outlier) were <1.1 ‰, less than the differences measured between the $\delta^{13}C$ of leaf, wood, and root tissues from the same plant (Heaton 1999).

In the Holocene the $\delta^{13}C$ of sedimentary organic carbon became progressively higher. The standard deviation (1.12) and coefficient of variance (5%) remained similar to glacial values, suggesting gradual change within the watershed. Prior to 4.3 ky BP, the greatest difference between sampled horizons was 2.2 ‰ and the average difference between samples was 0.2 ‰. The 4.3 ky BP sampling position marked the single largest $\delta^{13}C$ difference between horizons ($+4.16$ ‰). The interval from 4.3 ky to 500 years BP was a dynamic period exhibiting two distinct trends. $\delta^{13}C$ values between sampling horizons decline steeply from a high of -19.47 ‰ at 4.3 ky BP to a low of -24.9 ‰ at 1.5 ky BP. This trend reversed course 1.2 ky BP, becoming progressively higher and reaching -15.29 ‰ in the most recent sample radiocarbon dated to 500 years BP.

This record suggests that Holocene climate change allowed the encroachment of tropical grasses, sedges, and wetland plants. C_4 plants are more efficient with respect to light and water and are advantaged when conditions become arid (Schulze et al., 1996). If moisture is not a limiting factor, C_4 plants are favored by a warming climate (Collatz et al. 1998) which could indicate that temperature or sunlight change was significant exiting the last glacial stadial. From 5.2 to 1.2 ky BP the Fajardo floodplain indicated a shift favoring the abundance of C_3 type plants that might have been driven by Holocene climate fluctuations. Cooling temperatures at the end of the Holocene Thermal Maximum (~10–5 ky BP) were inferred from the Caricao Basin sediments (Haug et al., 2011) off the northern coast of Venezuela. Increased precipitation was recorded in a speleothem from central Puerto Rico (Rivera-Collazo et al., 2015) and from a pollen assemblage in Lake Valencia, Venezuela, ~2° east and ~8° south of Rio Fajardo (Bradbury et al., 1981; Leyden 2009). The difference between the samples dated at 860- and 500-years BP was $+4.12$ ‰ - the second largest difference between sampled horizons in the entire record. This change may be attributable to the introduction of agriculture and the expansion of grasses in the watershed as a result of anthropogenic activities. It could also reflect decreased precipitation during the Little Ice Age, recorded in the Caricao Basin off the northern coast of Venezuela (Haug et al., 2011).

Catastrophic events impact above ground biomass, successional growth patterns, litter fall/decomposition, and nutrient cycling. These processes before and after major storms have been quantified in the Luquillo Experimental Forest (Scatena et al., 1996; Zimmerman et al, 1995, 2014; Silver et al. 2014). Hurricane Hugo reduced above ground biomass and nutrient pools of N, P, K, Ca, and Mg by ~50% and generated a pulse of litter ~400 times daily background inputs (Lodge et al., 1991) affecting the quantity and quality of carbon in fluvial transport (Wohl and Ogden 2013; McDowell and Asbury 1994). In the forest today, the recurrence interval of major disturbance events is shorter than the recovery time of biomass and soil nutrient pools (Lugo and Scatena 1996). Massive growth pulses occur after hurricane events, however, the ecosystem does not attain steady state with respect to biomass or soil nutrients and always retains biomass volume below its support capacity (Sanford et al., 1991; Scatena et al., 1996). Nutrient cycles and ecosystem structure in the Luquillo Mountains today are specifically adapted to a disturbance regime (Lodge et al. 1994; Scatena et al., 2012).

In the wake of a hurricane, forest stand defoliation, breakage, and uprooting opens the canopy, and creates niche sites that successional species occupy (Brokaw 1998). Landslides also open the canopy to successional growth (Taylor et al., 1995). Ferns, palms, and woody shrubs are the dominant successional plants following hurricanes (e.g. *Cecroppia schreberiana, Guarea glabra*) (Brokaw, 1998; Lugo et al., 1998; Scatena et al., 1996). These trees have fast growth habits and rapidly consume nutrients deposited on the forest floor (Zimmerman et al., 1995). They close openings in the canopy quickly and prevent the encroachment of grasses in the forest, as commonly occurs in other disturbed ecosystems (Brokaw

Table 6
Ecological changes over the Fajardo floodplain stratigraphic record.

Time Frame	Date range[a] ky BP	Average $\delta^{13}C$	Standard deviation ‰	Coefficient of variance	Minimum $\delta^{13}C$	Maximum $\delta^{13}C$
Mid-Holocene to present	0–4.3	−20.8	2.74	13%	−24.97	−15.29
Early Holocene	5.2–11.7	−23.29	1.12	5%	−24.37	−21.14
Glacial	12.7–25.9	−26.23	1.23	5%	−29.72	−24.75
Holocene[b]	11.7–0.5	−22.64	1.84	8%	−24.97	−19.47
Glacial[c]	13–26	−25.94	0.67	3%	−27.1	−24.75

[a] Date ranges are delineated at the calibrated radiocarbon ages of sampled horizons (see Table 3).
[b] Holocene values as a whole, with the 500 yr BP samples removed.
[c] Pleistocene values considered with the minimum (−29.72) removed as an outlier.

and Grear 1991). Considering the $\delta^{13}C$ pattern in the Fajardo floodplain record, it is plausible that the onset of a hurricane-driven disturbance ecology caused the depletion of $\delta^{13}C$ ratios. Hurricane defoliation is greater on mountain slopes than in lowlands, which would increase the relative load of forest litter and woody debris in the stream channel (Brokaw and Grear 1991). These successional species are C_3-photosynthesizers, so their abundance will also cause a decreasing trend in $\delta^{13}C$. In the recent history of land cover change in the Fajardo watershed, researchers observed the rapid colonization of abandoned pasture by pioneer trees (Lugo and Helmer 2004; Lugo 2004). Taking these abandoned agricultural plots as disturbance analogues, trees have a competitive advantage even in parts of the landscape that are suitable for the growth of tropical grasses.

The $\delta^{13}C$ values measured 500 years ago likely reflect the biomass of agricultural crops, especially sugar cane, and grasslands enhanced by clearing land for pasture. It is possible that humans influenced the ecological composition of the watershed prior to colonization. People living in Puerto Rico used fire for land clearance and crop cultivation as early as 3.3 ky BP (Ramos et al., 2013; Pagán-Jiménez et al., 2015). Fire and/or agriculture should make the bulk $\delta^{13}C$ ratios higher. Within the time frame of pre-colonial occupation, anthropogenic influence could most reasonably be invoked for the 860-year-old sample, which reverses the trend in the $\delta^{13}C$ record. However, the $\delta^{13}C$ value of (-21.39 $^{o}/_{oo}$) is very close to the mean value of the Holocene $\delta^{13}C$ distribution. It is hard to attribute these changes to human occupation without additional evidence of inhabitation in the watershed. Most pre-colonial settlements in Puerto Rico were established on the coast and relied on marine resources. The Luquillo Mountains were a sacred place and there are signs of ceremonial practice within the forest (Scatena, 1989). It is most likely that pre-colonial occupation did not significantly disrupt the ecosystem in the watershed.

6. Conclusions

Records of terrestrial change in the Rio Fajardo watershed confirm that the ecosystem composition and rates of geomorphic processes have changed in response to climate forcing over the past 25 ky period. Erosion rates track the trends in precipitation over time and tend to remain stable within timeframes. Vegetation dynamics reveal a shift in abundance between C_3 and C_4 photosynthesizing plant groups that may be more strongly influenced by trends in temperature than in precipitation. Both systems appear to maintain a dynamic equilibrium with climate forcing through the Pleistocene-to-Holocene transition and during the Holocene prior to 5 ky BP. Paleoclimate proxies suggest that approximately 5 ky BP the Caribbean climate changed to a regime characterized by frequent, intense tropical storms. Our proxies for vegetation and erosion rate within the Fajardo watershed apparently transition to a state of pulsed response to disturbances at this time, evidenced by the degree of inter-sample variability and the overall magnitude of change. Studies of impacts from large, contemporary storms suggest that perturbation-response characteristics explain the magnitude and rate of geomorphic processes and cycling of biomass and nutrient pools in the Luquillo Mountains. The greatest anomaly in both records, however, is caused by colonial anthropogenic activity. This suggests that anthropogenic disruption of ecological and geomorphic systems can drive change that significantly exceeds the rate and magnitude of natural disturbance.

Author contributions

Emma J. Harrison: Writing – original draft, Visualization, Data curation, Formal analysis; Jane K. Willenbring: Fieldwork – sampling, Lab work – sample processing and analyses, Writing – review & editing, Supervision, Funding acquisition, Resources; Gilles Y. Brocard: Fieldwork – sediment sampling, Investigation, Writing – review & editing.

Declaration of competing interest

The authors declare that they have no known competing financial interests or personal relationships that could have appeared to influence the work reported in this paper.

Acknowledgements

Research reported in this publication was supported by the National Science Foundation (NSF) CAREER grant (1651243) to Jane Willenbring. It was also supported by the NSF -funded Luquillo Critical Zone Observatory (LCZO; EAR-1331841) grant. We thank the University of Pennsylvania for providing the facilities and instrumentation necessary for this work as well as Kirstin Washington, Art Johnson and Matthew Mellon. Isabel Rivera-Collazo is thanked for imparting her knowledge of the pre-colonial archaeological record in Puerto Rico.

References

Aalto, Rolf, Maurice-Bourgoin, Laurence, Dunne, Thomas, Montgomery, David R., Nittrouer, Charles A., Guyot, Jean Loup, 2003. Episodic sediment accumulation on amazonian flood plains influenced by El niño/southern oscillation. Nature 425 (6957), 493–497. https://doi.org/10.1038/nature02002.
Aide, T.M., Zimmerman, Jess K., Herrera, L., Rosario, M., I Serrano, Mayra, 1995. Forest recovery in abandoned tropical pastures in Puerto Rico. For. Ecol. Manag. 77, 77–86.
Aide, T.M., Zimmerman, Jess K., Rosario, M., Marcano-Vega, Humfredo, 1996. Forest recovery in abandoned cattle pastures along an elevational gradient in northeastern Puerto Rico. Biotropica 28 (4), 537–548.
Aide, T.M., Zimmerman, Jess K., Pascarella, John B., Rivera, Luis, Marcano-Vega, Humfredo, 2000. Forest regeneration in a chronosequence of tropical abandoned pastures: implications for restoration ecology. Restor. Ecol. 8 (4), 328–338. https://doi.org/10.1046/j.1526-100X.2000.80048.x.
Angeles, M.E., Gonzales, J.E., Erickson, D.J., Hernandez, J.L., 2007. Predictions of future climate change in the caribbean region using global general circulation models. Int. J. Climatol. 27, 555–569. https://doi.org/10.1002/joc.
Ashmore, P., 1991. Channel morphology and bed load pulses in braided, gravel-bed streams. Geografiska Annaler, Series A 73 A (1), 37–52. https://doi.org/10.1080/04353676.1991.11880331.
Aslan, Andres, Autin, Whitney J., 1999. Evolution of the Holocene Mississippi river floodplain, ferriday, Louisiana: insights on the origin of fine-grained floodplains. J. Sediment. Res. 69 (4), 800–815. https://doi.org/10.2110/jsr.69.800.
Balco, Greg, Briner, Jason, Finkel, R.C., Rayburn, John A., Ridge, John C., Schaefer, Joerg M., 2009. Regional beryllium-10 production rate calibration for late-glacial northeastern North America. Quat. Geochronol. 4 (2), 93–107. https://doi.org/10.1016/j.quageo.2008.09.001.
Bawiec, Walter J., 1999. Geology, Geochemistry, Geophysics, Mineral Occurrences and Mineral Resource Assessment for the Commonwealth of Puerto Rico. U.S. Geological Survey Open-File Report 98-038. http://pubs.usgs.gov/of/1998/of98-038/.
Berger, W.H., Vincent, E., Thierstein, H.R., 1981. The deep sea record major steps IN cenozoic ocean evolution. Society of Economic Paleontologists and Mineralogists 32, 489–504.
Bird, M.I., Fyfe, W.S., Pinheiro-Dick, D., Chivas, A.R., 1992. Partly deforested catchment. Global Biogeochem. Cycles 6 (3), 293–306.
Blanckenburg, Friedhelm von, 2005. The control mechanisms of erosion and weathering at basin scale from cosmogenic nuclides in river sediment. Earth Planet Sci. Lett. 237 (3–4), 462–479. https://doi.org/10.1016/j.epsl.2005.06.030.
Blanckenburg, Friedhelm von, Bouchez, J., Hella, Wittmann, 2012. Earth surface erosion and weathering from the 10Be (Meteoric)/9Be ratio. Earth Planet Sci. Lett. 351–352 (October), 295–305. https://doi.org/10.1016/j.epsl.2012.07.022.
Boschi, Vanessa, Willenbring, Jane K., 2021. Chemical and physical drivers of beryllium retention in two soil endmembers. Sci. Total Environ. 754, 141591. https://doi.org/10.1016/j.scitotenv.2020.141591.
Bouchez, J., Beyssac, Olivier, Galy, Valier, Gaillardet, Jérôme, France-Lanord, Christian, Maurice, Laurence, Moreira-Turcq, Patricia, 2010. Oxidation of petrogenic organic carbon in the amazon floodplain as a source of atmospheric CO2. Geology 38 (3), 255–258. https://doi.org/10.1130/G30608.1.
Boye, Kristin, Vincent, Noël, Tfaily, Malak M., Bone, Sharon E., Williams, Kenneth H., Bargar, John R., Scott, Fendorf, 2017. Thermodynamically controlled

preservation of organic carbon in floodplains. Nat. Geosci. 10 (6), 415–419. https://doi.org/10.1038/ngeo2940.

Bradbury, J. Platt, 1997. Sources of glacial moisture in mesoamerica. Quat. Int. 43–44 (97), 97–110.

Bradbury, J. Platt, Leyden, Barbara W., Salgado-Labouriau, M., Lewis, W.M., Schubert, C., Binford, M.W., Frey, D.G., Whitehead, D.R., Weibezahn, F.H., 1981. Late quaternary environmental history of Lake Valencia, Venezuela. Science 214 (4527). https://doi.org/10.1126/science.214.4527.1299, 1299 LP – 1305.

Brokaw, N., 1998. Cecropia schreberiana in the Luquillo mountains of Puerto Rico. Review Literature And Arts Of The Americas 64 (JUNE), 91–120.

Brokaw, N., Jason, S Grear, 1991. Forest structure before and after hurricane Hugo at three elevations in the Luquillo mountains , Puerto Rico. Biotropica 23 (4), 317–323.

Brown, Erik T., Stallard, Robert F., Larsen, Matthew C., Raisbeck, Grant M., Yiou, Françoise, 1995. Denudation rates determined from the accumulation of in situ-produced 10Be in the Luquillo experimental forest, Puerto Rico. Earth Planet Sci. Lett. 129 (1–4), 193–202. https://doi.org/10.1016/0012-821X(94)00249-X.

Burney, David A., Burney, Lida Pigott, MacPhee, R.D.E., 1994. Holocene charcoal stratigraphy from laguna tortuguero, Puerto Rico, and the timing of human arrival on the island. J. Archaeol. Sci. 21 (2), 273–281. https://doi.org/10.1006/jasc.1994.1027.

Cai, D.L., Tan, Francis C., Edmond, J.M., 1988. "Sources and transport of particulate organic carbon in the amazon river and estuary." *estuarine*. Coastal and Shelf Science 26 (1), 1–14. https://doi.org/10.1016/0272-7714(88)90008-X.

Campbell, Jayaka, Taylor, Michael A., Stephenson, Tannecia S., Watson, Rhodene A., Whyte, Felicia S., 2011. Future climate of the caribbean from a regional climate model. Int. J. Climatol. 31 (12), 1866–1878. https://doi.org/10.1002/joc.2200.

Clark, J.J., Wilcock, Peter R., 2000. Effects of land-use change on channel morphology in northeastern Puerto Rico. Bull. Geol. Soc. Am. 112 (12), 1763–1777. https://doi.org/10.1130/0016-7606(2000)112<1763:EOLUCO>2.0.CO;2.

Clement, A.C., Seager, R., Cane, M.A., 2000. "Suppression of El Niño during the mid-holocene by changes in the Earth's orbit. Paleoceanography 15 (6), 731–737. https://doi.org/10.1029/1999PA000466.

Collatz, G James, Berry, A., Clark, James S., 1998. Effects of climate and atmospheric CO2 partial pressure on the global distribution of C4 grasses: present, past, and future. Oecologia 114, 441–454.

Collins, D.B.G., Bras, R.L., Tucker, Gregory E., 2004. Modeling the effects of vegetation-erosion coupling on landscape evolution. J. Geophys. Res. 109 (F3), 1–11. https://doi.org/10.1029/2003jf000028.

DiBiase, Roman A., Whipple, Kelin X., 2011. The influence of erosion thresholds and runoff variability on the relationships among topography, climate, and erosion rate. J. Geophys. Res.: Earth Surface 116 (4), 1–17. https://doi.org/10.1029/2011JF002095.

Dixon, Jean L., Heimsath, Arjun M., James, Kaste, Amundson, Ronald, 2009. Climate-driven processes of hillslope weathering. Geology 37 (11), 975–978. https://doi.org/10.1130/G30045A.1.

Dominy, C.S., Haynes, R.J., Van Antwerpen, R., 2002. Loss of soil organic matter and related soil properties under long-term sugarcane production on two contrasting soils. Biol. Fertil. Soils 36 (5), 350–356. https://doi.org/10.1007/s00374-002-0538-5.

Donnelly, Jeffrey P., Woodruff, Jonathan D., 2007. Intense hurricane activity over the past 5,000 Years controlled by El Niño and the west african monsoon. Nature 447 (7143), 465–468. https://doi.org/10.1038/nature05834.

Dosseto, A., Buss, Heather L., Suresh, P.O., 2012. Rapid regolith formation over volcanic bedrock and implications for landscape evolution. Earth Planet Sci. Lett. 337–338 (July), 47–55. https://doi.org/10.1016/j.epsl.2012.05.008.

Farquhar, G.D., Ehleringer, J.R., Hubick, K.T., 1989. Carbon isotope discrimination and photosynthesis. Annu. Rev. Plant Physiol. Plant Mol. Biol. 40, 503–537.

Fensterer, Claudia, Scholz, Denis, Hoffmann, Dirk L., Spötl, Christoph, Schröder-Ritzrau, Andrea, Horn, Christian, Pajón, Jesus M., Mangini, Augusto, 2013. Millennial-scale climate variability during the last 12.5ka recorded in a caribbean speleothem. Earth Planet Sci. Lett. 361 (January), 143–151. https://doi.org/10.1016/j.epsl.2012.11.019.

Ferrier, Ken L., Taylor Perron, J., Mukhopadhyay, Sujoy, Rosener, Matt, Stock, Jonathan D., Huppert, Kimberly L., Slosberg, Michelle, 2013. "Covariation of climate and long-term erosion rates across a steep rainfall gradient on the Hawaiian island of kaua'i. Bull. Geol. Soc. Am. 125 (7–8), 1146–1163. https://doi.org/10.1130/B30726.1.

Fischer, Joseph C von, Tieszen, Larry L., 1995. Carbon isotope characterization of vegetation and soil organic matter in subtropical forests in Luquillo , Puerto Rico. Biotropica 27 (2), 138–148. http://www.jstor.org/stable/2388989.

Franklin, Janet, Serra-Diaz, Josep M., Syphard, Alexandra D., Regan, Helen M., 2016. Global change and terrestrial plant community dynamics. Proc. Natl. Acad. Sci. Unit. States Am. 113 (14), 3725–3734. https://doi.org/10.1073/pnas.1519911113.

Galy, Valier, France-Lanord, Christian, Lartiges, Bruno, 2008. Loading and fate of particulate organic carbon from the himalaya to the ganga-brahmaputra delta. Geochem. Cosmochim. Acta 72 (7), 1767–1787. https://doi.org/10.1016/j.gca.2008.01.027.

Gardner, L.R., Michener, W.K., Blood, E.R., Williams, T.M., Lipscomb, D.J., Jefferson, W.H., 1992. Ecological impact of hurricane Hugo - salinization of a coastal forest. Journal of Coastal Research, Special Issue 8 (8), 301–317.

Giannini, A., Cane, M.A., Kushnir, Y., 2001. Interdecadal changes in the ENSO teleconnection to the caribbean region and the north atlantic oscillation. J. Clim. 14 (13), 2867–2879. https://doi.org/10.1175/1520-0442(2001)014<2867:ICITET>2.0.CO;2.

Giry, Cyril, Felis, Thomas, Martin, Kölling, Scholz, Denis, Wei, Wei, Lohmann, Gerrit, Sander Scheffers, 2012. Mid- to late Holocene changes in tropical atlantic temperature seasonality and interannual to multidecadal variability documented in southern caribbean corals. Earth Planet Sci. Lett. 331–332, 187–200. https://doi.org/10.1016/j.epsl.2012.03.019.

González, Luis A., Gómez, Roger, 2002. High resolution speleothem paleoclimatology of northern Venezuela: a progress report. Bol. Soc. Venezolana Espel. 36, 27–29.

Graly, Joseph, Bierman, Paul R., Reusser, Lucas J., Pavich, Milan J., 2010. Meteoric 10Be in soil profiles - a global meta-analysis. Geochem. Cosmochim. Acta 74 (23), 6814–6829. https://doi.org/10.1016/j.gca.2010.08.036.

Graly, Joseph, Reusser, Lucas J., Bierman, Paul R., 2011. Short and long-term delivery rates of meteoric 10Be to terrestrial soils. Earth Planet Sci. Lett. 302 (3–4), 329–336. https://doi.org/10.1016/j.epsl.2010.12.020.

Harnois, Luc, 1988. The CIW index: a new chemical index of weathering. Sediment. Geol. 55 (3–4), 319–322. https://doi.org/10.1016/0037-0738(88)90137-6.

Haslett, John, Parnell, Andrew, 2008. A simple monotone process with application to radiocarbon-dated depth chronologies. J. Roy. Stat. Soc. C Appl. Stat. 57 (4), 399–418. https://doi.org/10.1111/j.1467-9876.2008.00623.x.

Haug, Gerald H., Hughen, Konrad A., Sigman, Daniel M., Peterson, Larry C., Ursula, Ro, 2011. Southward migration of the intertropical convergence Zone through the Holocene. Science 1304 (2001), 1304–1309. https://doi.org/10.1126/science.1059725.

Heaton, Tim H.E., 1999. Spatial, species, and temporal variations in the 13C/12C ratios of C3 plants: implications for palaeodiet studies. J. Archaeol. Sci. 26 (6), 637–649. https://doi.org/10.1006/jasc.1998.0381.

Hedges, John I., Turin, H.J., Ertel, John R., 1984. Sources and distributions of sedimentary organic matter in the columbia river drainage basin, Washington and Oregon. Limnol. Oceanogr. 29 (1), 35–46. https://doi.org/10.4319/lo.1984.29.1.0035.

Hedges, John I., Mayorga, Emilio, Tsamakis, Elizabeth, McClain, Michael E., Anthony, Aufdenkampe, Quay, Paul D., Richey, Jeffrey E., et al., 2000. Organic matter in Bolivian tributaries of the amazon river: a comparison to the lower mainstream. Limnol. Oceanogr. 45 (7), 1449–1466. https://doi.org/10.4319/lo.2000.45.7.1449.

Heikkilä, U., von Blanckenburg, Friedhelm, 2015. The global distribution of Holocene meteoric 10Be fluxes from atmospheric models. Distribution Maps for Terrestrial Earth Surface Applications." GFZ Data Services 10.

Heikkilä, U., Beer, J., Abreu, J.A., Steinhilber, F., 2013. On the atmospheric transport and deposition of the cosmogenic radionuclides (10Be): a review. Space Sci. Rev. https://doi.org/10.1007/s11214-011-9838-0.

Herman, Frederic, Champagnac, Jean-Daniel, 2015. "Plio-Pleistocene increase of erosion rates in mountain belts in response to climate change. Terra. Nova 28 (1). https://doi.org/10.1111/ter.12186.

Hobgood, Jay S., Cerveny, Randall S., 1988. Ice-age hurricanes and tropical storms. Nature 333 (6170), 243–245. https://doi.org/10.1038/333243a0.

Hodell, David A., Curtis, Jason, Jones, Glenn, Higuera-Gundy, Antonia, Brenner, M., Binford, Michael, Dorsey, Kathleen, 1991. Reconstruction of caribbean climate change over the past 10,500 years. Nature 352, 790–793.

Homer, C.C. Huang, Yang, L., Wylie, B., Coan, M., 2004. Development of a 2001 national landcover database for the United States. Photogramm. Eng. Rem. Sens. 70 (7), 829–840.

Huang, Y., Street-Perrott, F.A., Metcalfe, S.E., Brenner, M., Moreland, M., Freeman, K.H., 2001. Climate change as the dominant control on glacial-interglacial variations in C3 and C4 plant abundance. Science 293 (5535), 1647–1651. https://doi.org/10.1126/science.1060143.

Islebe, Gerald A., Hooghiemstra, Henry, Brenner, M., Curtis, Jason, Hodell, David A., 1996. A Holocene vegetation history from lowland Guatemala. Holocene 6 (3), 265–271. https://doi.org/10.1177/095968369600600302.

Jagercikova, M., Cornu, S., Bourlès, D., Antoine, P., Mayor, M., Guillou, V., 2015. Understanding long-term soil processes using meteoric 10 Be: a first attempt on loessic deposits. Quat. Geochronol. 27 (April), 11–21. https://doi.org/10.1016/j.quageo.2014.12.003.

Jerolmack, Douglas J., Sadler, Peter, 2007. Transience and persistence in the depositional record of continental margins. J. Geophys. Res.: Earth Surface 112 (3), 1–14. https://doi.org/10.1029/2006JF000555.

Jungers, Matthew C., Bierman, Paul R., Matmon, Ari, Nichols, Kyle, Larsen, Jennifer, Finkel, R.C., 2009. Tracing hillslope sediment production and transport with in situ and Meteoric^{10}Be. J. Geophys. Res.: Earth Surface 114 (4). https://doi.org/10.1029/2008JF001086.

Karmalkar, Ambarish V., Taylor, Michael A., Campbell, Jayaka, Stephenson, Tannecia S., New, Mark, Abel, Centella, Benzanilla, Arnoldo, Charlery, John, 2013. A review of observed and projected changes in climate for the islands in the caribbean. Atmósfera 26 (2), 283–309. https://doi.org/10.1016/S0187-6236(13)71076-2.

Koch, Alexander, Brierley, Chris, Maslin, Mark M., Lewis, Simon L., 2019. Earth system impacts of the European arrival and great dying in the americas after 1492. Quat. Sci. Rev. 207, 13–36. https://doi.org/10.1016/j.quascirev.2018.12.004.

Kohn, Matthew J., 2010. Carbon isotope compositions of terrestrial C3 plants as indicators of (Paleo)Ecology and (paleo). Climate 107 (46). https://doi.org/10.1073/pnas.1004933107/-/DCSupplemental.

Lal, D., Peters, B., 1967. Cosmic ray produced radioactivity on the Earth. In: HANDBOOK OF PHYSICS, vol. 46. KOSMISCHE STRAHLUNG, pp. 551–612. https://doi.org/10.1007/978-3-642-46079-1_7.

Larsen, Matthew C., Torres Sanchez, A.J., 1992. Landslides triggered by hurricane Hugo in eastern Puerto Rico, september 1989. Caribb. J. Sci. 28 (3–4), 113–125.
Larsen, Matthew C., Torres-Sánchez, Angel J., 1998. The frequency and distribution of recent landslides in three montane tropical regions of Puerto Rico. Geomorphology 24 (4), 309–331.
Larsen, Matthew C., Torres-Sánchez, Angel J., Concepción, Iris M., 1999. Slopewash, surface runoff and fine-litter transport in forest and landslide scars in humid-tropical steeplands, Luquillo experimental forest, Puerto Rico. Earth Surf. Process. Landforms 24 (6), 481–502. https://doi.org/10.1002/(SICI)1096-9837(199906)24:6<481::AID-ESP967>3.0.CO;2-G.
Lewis, D.W., McConchie, D., 1994. Textures. In: Analytical Sedimentology, 92–129. Springer, Boston, Massachusetts.
Leyden, Barbara W., 2009. "Late quaternary aridity and Holocene moisture fluctuations in the Lake Valencia basin , Venezuela author (s). In: Barbara, W. (Ed.), Leyden Published By : Ecological Society of America Stable. Http://Www.Jstor.Org/Stable/1939181 LATE QUATERNARY ARIDITY AND HO." America 66 (4): 1279–95.
Leyden, Barbara W., Brenner, M., Hodell, David A., Curtis, Jason, 1994. Orbital and internal forcing of climate on the yucatan peninsula for the past ca. 36 ka. Palaeogeogr. Palaeoclimatol. Palaeoecol. 109 (2–4), 193–210. https://doi.org/10.1016/0031-0182(94)90176-7.
Lisiecki, Lorraine E., Raymo, Maureen E., 2005. A pliocene-pleistocene stack of 57 globally distributed benthic D18O records. Paleoceanography 20 (1), 1–17. https://doi.org/10.1029/2004PA001071.
Lodge, Jean D., McDowell, William H., 1991. Summary of ecosystem-level effects of caribbean hurricane. Biotropica 23 (4), 373–378.
Lodge, Jean D., Scatena, Frederick N., Asbury, C.E., Sanchez, M.J., 1991. Fine litterfall and related nutrient inputs resulting from hurricane Hugo in subtropical Wet and lower montane rain forests of Puerto Rico. Biotropica 23 (4a), 336–342.
Lodge, Jean D., McDowell, William H., McSwiney, C.P., 1994. The importance of nutrient pulses in tropical forests. Trends Ecol. Evol. 9 (10), 384–387. https://doi.org/10.1016/0169-5347(94)90060-4.
Louchouarn, Patrick, Lucotte, Marc, Canuel, René, Gagné, Jean Pierre, Richard, Louis Filip, 1997. Sources and early diagenesis of lignin and bulk organic matter in the sediments of the lower st. Lawrence estuary and the saguenay fjord. Mar. Chem. 58 (1–2), 3–26. https://doi.org/10.1016/S0304-4203(97)00022-4.
Louchouarn, Patrick, Lucotte, Marc, Farella, Nicolina, 1999. Historical and geographical variations of sources and transport of terrigenous organic matter within a large-scale coastal environment. Org. Geochem. 30 (7), 675–699. https://doi.org/10.1016/S0146-6380(99)00019-4.
Lugo, Ariel E., 2004. The outcome of alien tree invasions in Puerto Rico. Front. Ecol. Environ. 2 (5), 265–273. https://doi.org/10.1890/1540-9295(2004)002[0265:TOOATI]2.0.CO;2.
Lugo, Ariel E., Helmer, Eileen, 2004. "Emerging forests on abandoned land: Puerto Rico's new forests. For. Ecol. Manag. 190 (2–3), 145–161. https://doi.org/10.1016/j.foreco.2003.09.012.
Lugo, Ariel E., Scatena, Frederick N., 1996. Background and catastrophic tree mortality in tropical moist , Wet , and rain forests. Biotropica 28 (4), 585–599.
Lugo, Ariel E., Francis, John K., Frangi, Jorge L., 1998. Prestoea Montana (R. Graham) Nichols. Sierra Palm. Palmaceae. Palm Family." *Rio Piedras, Puerto Rico*, vol. 9. US Department of Agriculture, Forest Service, International Institute of Tropical Forestry (SO-IT).
Lyell, Charles, Deshayes, Gerard Paul, 1830. Principles of Geology: Being an Attempt to Explain the Former Changes of the Earth's Surface by References to Causes Now in Operation.
Marin-Spiotta, Erika, Silver, Whendee L., Swanston, Christopher W., Ostertag, Rebecca, 2009. Soil organic matter dynamics during 80 Years of reforestation of tropical pastures. Global Change Biol. 15 (6), 1584–1597. https://doi.org/10.1111/j.1365-2486.2008.01805.x.
Marshall, Jill A., Roering, Joshua J., Bartlein, Patrick J., Gavin, Daniel G., Granger, Darryl E., Rempel, Alan W., Praskievicz, Sarah J., Hales, Tristram C., 2015. Frost for the trees: did climate increase erosion in unglaciated landscapes during the late Pleistocene? Science Advances 1 (10). https://doi.org/10.1126/sciadv.1500715.
McDowell, William H., Asbury, C.E., 1994. Export of carbon, nitrogen, and major ions from three tropical montane watersheds. Limnol. Oceanogr. https://doi.org/10.4319/lo.1994.39.1.0111.
Medina, Ernesto, Sternberg, Leonel, Cuevas, Elvira, 1991. Vertical stratification of °13C values in closed natural and plantation forests in the Luquillo mountains, Puerto Rico. Oecologia 87 (3), 369–372. https://doi.org/10.1007/BF00634593.
Medina, Ernesto, Martinelli, Luiz, Victoria Barbosa, Edelcilio, Luiz Victoria, Reynaldo, 1999. Natural abundance of 13C in tropical grasses from the INPA, instituto nacional de Pesquisas da amazônia, herbarium. Rev. Bras. Botânica 22 (1), 44–51. https://doi.org/10.1590/s0100-84041999000100007.
Mellon, M.T., 2000. Records of Pleistocene Terrestrial Climate Changes in Puerto Rico Archived in Stacked Paleosols. University of Pennsylvania.
Metcalfe, S.E., Bimpson, A., Courtice, A.J., O'Hara, S.L., Taylor, D.M., 1997. Climate change at the monsoon/westerly boundary in northern Mexico. J. Paleolimnol. 17 (2), 155–171. https://doi.org/10.1023/A:1007905824147.
Meyer, David L., Bries, Jill M., Greenstein, Benjamin J., Debrot, Adolphe O., 2003. Preservation of in situ reef framework in regions of low hurricane frequency: Pleistocene of curaçao and bonaire, southern caribbean. Lethaia 36 (3), 273–286. https://doi.org/10.1080/00241160310004675.
Montgomery, David R., 2007. Soil erosion and agricultural sustainability. Proc. Natl. Acad. Sci. U. S. A 104 (33), 13268–13272. https://doi.org/10.1073/pnas.0611508104.
Moyer, Ryan P., Bauer, James E., Grottoli, Andréa G., 2013. Carbon isotope biogeochemistry of tropical small mountainous river, estuarine, and coastal systems of Puerto Rico. Biogeochemistry 112 (1–3), 589–612. https://doi.org/10.1007/s10533-012-9751-y.
Murphy, Sheila F., Stallard, Robert F., Scholl, Martha A., González, Grizelle, Torres-Sánchez, Angel J., 2017. Reassessing rainfall in the Luquillo mountains, Puerto Rico: local and global ecohydrological implications. PloS One 12 (7), 1–26. https://doi.org/10.1371/journal.pone.0180987.
Nishiizumi, K., Imamura, Mineo, Caffee, M.W., Southon, John R., Finkel, R.C., McAninch, Jeffrey, 2007. Absolute calibration of 10 Be AMS standards. Nucl. Instrum. Methods Phys. Res. Sect. B Beam Interact. Mater. Atoms 258 (2), 403–413. https://doi.org/10.1016/j.nimb.2007.01.297.
Norton, Kevin P., Schlunegger, Fritz, 2017. Lack of a weathering signal with increased cenozoic erosion? Terra. Nova 29 (5). https://doi.org/10.1111/ter.12278.
Onstad, Gretchen D., Canfield, Donald E., Quay, Paul D., Hedges, John I., 2000. Sources of particulate organic matter in rivers from the continental USA: lignin phenol and stable carbon isotope compositions. Geochem. Cosmochim. Acta 64 (20), 3539–3546. https://doi.org/10.1016/S0016-7037(00)00451-8.
Owen, Justine, Amundson, Ronald, Dietrich, W.E., Nishiizumi, K., Sutter, Brad, Chong, Guillermo, 2011. The sensitivity of hillslope bedrock erosion to precipitation. Earth Surf. Process. Landforms 36 (1), 117–135. https://doi.org/10.1002/esp.2083.
O'Leary, Marion H., 1988. Carbon isotopes in photosynthesis. Bioscience 38 (5), 328–336. https://doi.org/10.2307/1310735.
Pagán-Jiménez, Jaime R., Rodríguez-Ramos, Reniel, Reid, Basil A., van den Bel, Martijn, Corinne, L., Hofman, 2015. Early dispersals of maize and other food plants into the southern caribbean and northeastern south America. Quat. Sci. Rev. 123 (September), 231–246. https://doi.org/10.1016/j.quascirev.2015.07.005.
Parnell, A.C., Haslett, J., Allen, J.R.M., Buck, C.E., Huntley, B., 2008. A flexible approach to assessing synchroneity of past events using bayesian reconstructions of sedimentation history. Quat. Sci. Rev. 27 (19–20), 1872–1885. https://doi.org/10.1016/j.quascirev.2008.07.009.
Peten, Lowlands, Curtis, Jason, Brenner, M., Hodell, David A., Balser, Richard A., Islebe, Gerald A., Henry, Hooghiemstra, 1998. A multi-proxy study of Holocene environmental change in the maya. J. Paleolimnol. 19, 139–159. https://doi.org/10.1023/a:1007968508262.
Peterson, Larry C., Haug, Gerald H., 2006. Variability in the mean latitude of the atlantic intertropical convergence Zone as recorded by riverine input of sediments to the cariaco basin (Venezuela). Palaeogeogr. Palaeoclimatol. Palaeoecol. 234 (1), 97–113. https://doi.org/10.1016/j.palaeo.2005.10.021.
Pike, Andrew S., Scatena, Frederick N., Wohl, Ellen, 2010. Lithological and fluvial controls on the geomorphology of tropical montane stream channels in Puerto Rico. Earth Surf. Process. Landforms 35, 1402–1417. https://doi.org/10.1002/esp.1978.
Planavsky, Noah, Partin, Camille, Bekker, Andrey, 2016. Carbon isotopes as a geochemical tracer. In: Encyclopedia of Astrobiology, vols. 366–71. Springer Berlin Heidelberg. https://doi.org/10.1007/978-3-662-44185-5_228.
Ramos, Reniel Rodríguez, Jiménez, Jaime Pagán, Santiago-Blay, Jorge, Lambert, Joseph B., Craig, Patrick R., 2013. Some indigenous uses of plants in pre-columbian Puerto Rico. Life: The Excitement of Biology 1 (1), 83–90. https://doi.org/10.9784/leb1(1)rodriguez.09.
Reimer, Paula J., Austin, William E.N., Bard, Edouard, Bayliss, Alex, Blackwell, Paul G., Bronk Ramsey, Christopher, Martin, Butzin, et al., 2020. The IntCal20 northern hemisphere radiocarbon age calibration curve (0-55 cal KBP). Radiocarbon 62 (4), 725–757. https://doi.org/10.1017/RDC.2020.41.
Reiners, Peter W., Ehlers, Todd A., Mitchell, Sara G., Montgomery, David R., 2003. Coupled spatial variations in precipitation and long-term erosion rates across the Washington cascades. Nature 426 (6967), 645–647. https://doi.org/10.1038/nature02111.
Retallack, Gregory J., 2008. Soils of the Past: an Introduction to Paleopedology. John Wiley & Sons.
Reusser, Lucas J., Bierman, Paul R., 2010. Using meteoric 10Be to track fl uvial sand through the waipaoa river basin, New Zealand. Geology 38 (1), 47–50. https://doi.org/10.1130/G30395.1.
Rico, Puerto, Larsen, Matthew C., Simon, Andrew, 1993. A rainfall intensity-duration threshold for landslides in a humid-tropical environment. Source: Geogr. Ann. Phys. Geogr. 75.
Riebe, Clifford S., Kirchner, James W., Finkel, R.C., 2004. Erosional and climatic effects on long-term chemical weathering rates in granitic landscapes spanning diverse climate regimes. Earth Planet Sci. Lett. 224, 547–562. https://doi.org/10.1016/j.epsl.2004.05.019.
Rivera-Collazo, Isabel, C., Winter, Amos, Scholz, Denis, Mangini, Augusto, Miller, Thomas E., Kushnir, Yochanan, Black, David, 2015. Human adaptation strategies to abrupt climate change in Puerto Rico ca. 3.5 ka. Holocene 25 (4), 627–640. https://doi.org/10.1177/0959683614565951.
Rodbell, Donald T., Seltzer, Geoffrey O., Anderson, David M., Abbott, Mark B., Enfield, David B., Newman, Jeremy H., 1999. An ~15,000-Year record of El nino-driven alluviation in southwestern Ecuador. Science 283 (5401), 516–520. https://doi.org/10.1126/science.283.5401.516.
Salomé, Clémence, Nunan, Naoise, Pouteau, Valérie, Lerch, Thomas Z., Chenu, Claire, 2010. Carbon dynamics in topsoil and in subsoil may Be controlled by different regulatory mechanisms. Global Change Biol. 16 (1), 416–426. https://doi.org/10.1111/j.1365-2486.2009.01884.x.
Sandweiss, D.H., Richardson, J.B., Reitz, E.J., Rollins, H.B., Maasch, Kirk A., 1996.

Geoarchaeological evidence from Peru for a 5000 Years B.P. Onset of El Niño. Science 273 (5281), 1531–1533.
Sanford, R.L., Parton, William J., Ojima, Dennis S., Lodge, Jean D., 1991. “Hurricane effects on soil organic matter dynamics and forest production in the Luquillo experimental forest , Puerto Rico: results of simulation modeling. Biotropica 23 (4), 364–372.
Sarmiento, Jorge L., Gruber, Nicolas, 2002. Sinks for anthropogenic carbon. Phys. Today 55 (8), 30. https://doi.org/10.1063/1.1510279.
Scatena, Frederick N., 1989. An Introduction to the Physiography and History of the Bisley Experimental Watersheds in the Luquillo Mountains of Puerto Rico.
Scatena, Frederick N., Moya, S., Estrada, C., Chinea, J.D., 1996. The first five years in the reorganization of aboveground biomass and nutrient use following hurricane Hugo in the Bisley experimental watersheds , Luquillo experimental forest. Ecosystems 28 (4), 424–440.
Scatena, Frederick N., Blanco, J.F., Beard, K.H., Waide, R.B., Lugo, Ariel E., Brokaw, N., Silver, Whendee L., Haines, B.L., Zimmerman, Jess K., 2012. Disturbance regime. In: A Caribbean Forest Tapestry: the Multidimensional Nature of Disturbance and Response, vols. 164–200. Oxford University Press, New York.
Scheingross, Joel S., Hovius, N., Dellinger, M., Hilton, R.G., Repasch, M., Sachse, D., Gröcke, D.R., Vieth-Hillebrand, A., Turowski, Jens M., 2019. Preservation of organic carbon during active fluvial transport and particle abrasion. Geology 47 (10), 958–962. https://doi.org/10.1130/G46442.1.
Schulze, E.D., Ellis, R., Schulze, W., Trimborn, P., Ziegler, H., 1996. Diversity, metabolic types and Δ13C carbon isotope ratios in the grass flora of Namibia in relation to growth form, precipitation and habitat conditions. Oecologia 106 (3), 352–369. https://doi.org/10.1007/BF00334563.
Schumer, Rina, Jerolmack, Douglas J., 2009. Real and apparent changes in sediment deposition rates through time. J. Geophys. Res.: Solid Earth 114 (3), 1–12. https://doi.org/10.1029/2009JF001266.
Silver, Whendee L., Scatena, Frederick N., Johnson, A.H., Siccama, T.G., Sanchez, M.J., 1994. “Nutrient availability in a montane Wet tropical Forest : spatial patterns and methodological considerations. Plant Soil 164 (1), 129–145.
Silver, Whendee L., Hall, Steven J., González, Grizelle, 2014. Differential effects of canopy trimming and litter deposition on litterfall and nutrient dynamics in a Wet subtropical forest. For. Ecol. Manag. 332, 47–55. https://doi.org/10.1016/j.foreco.2014.05.018.
Singh, Arvind, Fienberg, Kurt, Jerolmack, Douglas J., Marr, Jeffrey, Foufoula-Georgiou, Efi, 2009. Experimental evidence for statistical scaling and intermittency in sediment transport rates. J. Geophys. Res.: Earth Surface 114 (1), 1–16. https://doi.org/10.1029/2007JF000963.
Smith, B.N., Epstein, S., 1971. Two categories of c/c ratios for higher plants. Plant Physiol. 47 (3), 380–384.
Stallard, Robert F., 2012. Weathering, Landscape Equilibrium, and Carbon in Four Watersheds in Eastern Puerto Rico: Chapter H in Water Quality and Landscape Processes of Four Watersheds in Eastern Puerto Rico.” No. 1789-H. *US Geological Survey*, No. 1789-H, pp. 199–248.
Swanson, Kathleen M., Watson, Elizabeth, Aalto, Rolf, Wesley Lauer, J., Bera, Marie T., Marshall, Andrew, Taylor, Mark P., Apte, Simon C., Dietrich, W.E., 2008. Sediment load and floodplain deposition rates: comparison of the fly and strickland rivers, Papua New Guinea. J. Geophys. Res.: Earth Surface 113 (1), 2–17. https://doi.org/10.1029/2006JF000623.
Tartaglione, Carissa A., Smith, Shawn R., O'Brien, James J., 2003. ENSO impact on hurricane landfall probabilities for the caribbean. J. Clim. 16 (17), 2925–2931. https://doi.org/10.1175/1520-0442(2003)016<2925:EIOHLP>2.0.CO;2.
Taylor, C.M., Silander, S., Waide, R.B., J Pfeiffer, W., 1995. Recovery of a tropical forest after gamma irradiation: a 23-year chronicle. In: Tropical Forests: Management and Ecology, 258–85. Springer, New York.
Thomlinson, John R., I Serrano, Mayra, Lopez, Tania M., Aide, T.M., Zimmerman, Jess K., 1996. Land-use dynamics in a post-agricultural Puerto Rican landscape (1936-1988). Biotropica 28 (4), 525–536.
Thurman, Earl Michael, 2012. Organic Geochemistry of Natural Waters, vol. 2. Springer Science & Business Media.
Tieszen, Larry L., 1991. Natural variations in the carbon isotope values of plants: implications for archaeology, ecology, and paleoecology. J. Archaeol. Sci. 18 (3), 227–248. https://doi.org/10.1016/0305-4403(91)90063-U.
Valletta, Rachel D., Willenbring, Jane K., Lewis, Adam R., Ashworth, Allan C., Caffee, M.W., 2015. Extreme decay of meteoric beryllium-10 as a proxy for persistent aridity. Sci. Rep. 5, 1–7. https://doi.org/10.1038/srep17813.
Willenbring, Jane K., von Blanckenburg, Friedhelm, 2010. Meteoric cosmogenic beryllium-10 adsorbed to river sediment and soil: applications for earth-surface dynamics. Earth Sci. Rev. https://doi.org/10.1016/j.earscirev.2009.10.008.
Willenbring, Jane K., Von Blanckenburg, Friedhelm, 2010. Long-term stability of global erosion rates and weathering during late-cenozoic cooling. Nature 465 (7295), 211–214. https://doi.org/10.1038/nature09044.
Willenbring, Jane K., Jerolmack, Douglas J., 2015. The null hypothesis: globally steady rates of erosion, weathering fluxes and shelf sediment accumulation during late cenozoic mountain uplift and glaciation. Terra. Nova 28 (1). https://doi.org/10.1111/ter.12185.
Wohl, Ellen, Ogden, Fred L., 2013. Organic carbon export in the form of wood during an extreme tropical storm, upper Rio chagres, Panama. Earth Surf. Process. Landforms 38 (12), 1407–1416. https://doi.org/10.1002/esp.3389.
Wolf, Jeffrey, Brocard, Gilles Y., Willenbring, Jane K., Porder, Stephen, Uriarte, María, 2016. Abrupt change in forest height along a tropical elevation gradient detected using airborne LiDAR. Rem. Sens. 8 (10), 1–10. https://doi.org/10.3390/rs8100864.
Wood, Tana E., González, Grizelle, Silver, Whendee L., Reed, Sasha C., Cavaleri, Molly A., 2019. On the shoulders of giants: continuing the legacy of large-scale ecosystem manipulation experiments in Puerto Rico. Forests 10 (3), 1–18. https://doi.org/10.3390/f10030210.
Woodruff, Jonathan D., Donnelly, Jeffrey P., Mohrig, David C., Geyer, Wayne R., 2008. Reconstructing relative flooding intensities responsible for hurricane-induced deposits from laguna playa grande, Vieques, Puerto Rico. Geology 36 (5), 391–394. https://doi.org/10.1130/G24731A.1.
You, Chen Feng, Lee, Typhoon, Yuan, Huei Li, 1989. The partition of Be between soil and water. Chem. Geol. 77 (2), 105–118. https://doi.org/10.1016/0009-2541(89)90136-8.
Zimmerman, Author J.K., Pulliam, W.M., Lodge, Jean D., Fetcher, N., Parrotta, J.A., Asbury, C.E., Walker, L.R., Waide, R.B., Zimmerman, J.K., 1995. Nitrogen immobilization by decomposing woody debris and the recovery of tropical Wet forest from hurricane damage. Oikos 72 (3), 314–322.
Zimmerman, Jess K., Aaron Hogan, James, Shiels, Aaron B., Bithorn, John E., Matta Carmona, Samuel, Brokaw, N., 2014. Seven-year responses of trees to experimental hurricane effects in a tropical rainforest, Puerto Rico. For. Ecol. Manag. 332, 64–74. https://doi.org/10.1016/j.foreco.2014.02.029.